EUROPEAN ORGANIZATION FOR NUCLEAR RESEARCH

CERN–EP/2003-018

11 April 2003

Study of the hadronic photon structure function at LEP2

DELPHI Collaboration

Abstract

The photon structure function F_2^γ has been studied at Q^2 from 3 GeV$^2/c^4$ to 2600 GeV$^2/c^4$. The data correspond to an integrated luminosity of 78 pb^{-1} at LEP1 and 548 pb^{-1} at LEP2, collected by the DELPHI detector during the 1994-1995 and 1996-2000 LEP runs respectively. Experimental distributions are compared with the predictions of various models. The procedure of F_2^γ extraction from the data and its uncertainty are discussed. The F_2^γ estimated from the fit of models to the data are compared with some theoretical expectations. A result for the Q^2 evolution of the photon structure function in different x intervals is presented.

J.Abdallah[25], P.Abreu[22], W.Adam[51], P.Adzic[11], T.Albrecht[17], T.Alderweireld[2], R.Alemany-Fernandez[8], T.Allmendinger[17], P.P.Allport[23], U.Amaldi[29], N.Amapane[45], S.Amato[48], E.Anashkin[36], A.Andreazza[28], S.Andringa[22], N.Anjos[22], P.Antilogus[27], W-D.Apel[17], Y.Arnoud[14], S.Ask[26], B.Asman[44], J.E.Augustin[25], A.Augustinus[8], P.Baillon[8], A.Ballestrero[46], P.Bambade[20], R.Barbier[27], D.Bardin[16], G.Barker[17], A.Baroncelli[39], M.Battaglia[8], M.Baubillier[25], K-H.Becks[53], M.Begalli[6], A.Behrmann[53], E.Ben-Haim[20], N.Benekos[32], A.Benvenuti[5], C.Berat[14], M.Berggren[25], L.Berntzon[44], D.Bertrand[2], M.Besancon[40], N.Besson[40], D.Bloch[9], M.Blom[31], M.Bluj[52], M.Bonesini[29], M.Boonekamp[40], P.S.L.Booth[23], G.Borisov[21], O.Botner[49], B.Bouquet[20], T.J.V.Bowcock[23], I.Boyko[16], M.Bracko[43], R.Brenner[49], E.Brodet[35], P.Bruckman[18], J.M.Brunet[7], L.Bugge[33], P.Buschmann[53], M.Calvi[29], T.Camporesi[8], V.Canale[38], F.Carena[8], N.Castro[22], F.Cavallo[5], M.Chapkin[42], Ph.Charpentier[8], P.Checchia[36], R.Chierici[8], P.Chliapnikov[42], J.Chudoba[8], S.U.Chung[8], K.Cieslik[18], P.Collins[8], R.Contri[13], G.Cosme[20], F.Cossutti[47], M.J.Costa[50], B.Crawley[1], D.Crennell[37], J.Cuevas[34], J.D'Hondt[2], J.Dalmau[44], T.da Silva[48], W.Da Silva[25], G.Della Ricca[47], A.De Angelis[47], W.De Boer[17], C.De Clercq[2], B.De Lotto[47], N.De Maria[45], A.De Min[36], L.de Paula[48], L.Di Ciaccio[38], A.Di Simone[39], K.Doroba[52], J.Drees[53,8], M.Dris[32], G.Eigen[4], T.Ekelof[49], M.Ellert[49], M.Elsing[8], M.C.Espirito Santo[22], G.Fanourakis[11], D.Fassouliotis[11,3], M.Feindt[17], J.Fernandez[41], A.Ferrer[50], F.Ferro[13], U.Flagmeyer[53], H.Foeth[8], E.Fokitis[32], F.Fulda-Quenzer[20], J.Fuster[50], M.Gandelman[48], C.Garcia[50], Ph.Gavillet[8], E.Gazis[32], R.Gokieli[8,52], B.Golob[43], G.Gomez-Ceballos[41], P.Goncalves[22], E.Graziani[39], G.Grosdidier[20], K.Grzelak[52], J.Guy[37], C.Haag[17], A.Hallgren[49], K.Hamacher[53], K.Hamilton[35], J.Hansen[33], S.Haug[33], F.Hauler[17], V.Hedberg[26], M.Hennecke[17], H.Herr[8], J.Hoffman[52], S-O.Holmgren[44], P.J.Holt[8], M.A.Houlden[23], K.Hultqvist[44], J.N.Jackson[23], G.Jarlskog[26], P.Jarry[40], D.Jeans[35], E.K.Johansson[44], P.D.Johansson[44], P.Jonsson[27], C.Joram[8], L.Jungermann[17], F.Kapusta[25], S.Katsanevas[27], E.Katsoufis[32], G.Kernel[43], B.P.Kersevan[8,43], A.Kiiskinen[15], B.T.King[23], N.J.Kjaer[8], P.Kluit[31], P.Kokkinias[11], C.Kourkoumelis[3], O.Kouznetsov[16], Z.Krumstein[16], M.Kucharczyk[18], J.Lamsa[1], G.Leder[51], F.Ledroit[14], L.Leinonen[44], R.Leitner[30], J.Lemonne[2], V.Lepeltier[20], T.Lesiak[18], W.Liebig[53], D.Liko[51], A.Lipniacka[44], J.H.Lopes[48], J.M.Lopez[34], D.Loukas[11], P.Lutz[40], L.Lyons[35], J.MacNaughton[51], A.Malek[53], S.Maltezos[32], F.Mandl[51], J.Marco[41], R.Marco[41], B.Marechal[48], M.Margoni[36], J-C.Marin[8], C.Mariotti[8], A.Markou[11], C.Martinez-Rivero[41], J.Masik[12], N.Mastroyiannopoulos[11], F.Matorras[41], C.Matteuzzi[29], F.Mazzucato[36], M.Mazzucato[36], R.Mc Nulty[23], C.Meroni[28], W.T.Meyer[1], E.Migliore[45], W.Mitaroff[51], U.Mjoernmark[26], T.Moa[44], M.Moch[17], K.Moenig[8,10], R.Monge[13], J.Montenegro[31], D.Moraes[48], S.Moreno[22], P.Morettini[13], U.Mueller[53], K.Muenich[53], M.Mulders[31], L.Mundim[6], W.Murray[37], B.Muryn[19], G.Myatt[35], T.Myklebust[33], M.Nassiakou[11], F.Navarria[5], K.Nawrocki[52], R.Nicolaidou[40], M.Nikolenko[16,9], A.Oblakowska-Mucha[19], V.Obraztsov[42], A.Olshevski[16], A.Onofre[22], R.Orava[15], K.Osterberg[15], A.Ouraou[40], A.Oyanguren[50], M.Paganoni[29], S.Paiano[5], J.P.Palacios[23], H.Palka[18], Th.D.Papadopoulou[32], L.Pape[8], C.Parkes[24], F.Parodi[13], U.Parzefall[8], A.Passeri[39], O.Passon[53], L.Peralta[22], V.Perepelitsa[50], A.Perrotta[5], A.Petrolini[13], J.Piedra[41], L.Pieri[39], F.Pierre[40], M.Pimenta[22], E.Piotto[8], T.Podobnik[43], V.Poireau[8], M.E.Pol[6], G.Polok[18], P.Poropat[47], V.Pozdniakov[16], N.Pukhaeva[2,16], A.Pullia[29], J.Rames[12], L.Ramler[17], A.Read[33], P.Rebecchi[8], J.Rehn[17], D.Reid[31], R.Reinhardt[53], P.Renton[35], F.Richard[20], J.Ridky[12], M.Rivero[41], D.Rodriguez[41], A.Romero[45], P.Ronchese[36], E.Rosenberg[1], P.Roudeau[20], T.Rovelli[5], V.Ruhlmann-Kleider[40], D.Ryabtchikov[42], A.Sadovsky[16], L.Salmi[15], J.Salt[50], A.Savoy-Navarro[25], U.Schwickerath[8], A.Segar[35], R.Sekulin[37], M.Siebel[53], A.Sisakian[16], G.Smadja[27], O.Smirnova[26], A.Sokolov[42], A.Sopczak[21], R.Sosnowski[52], T.Spassov[8], M.Stanitzki[17], A.Stocchi[20], J.Strauss[51], B.Stugu[4], M.Szczekowski[52], M.Szeptycka[52], T.Szumlak[19], T.Tabarelli[29], A.C.Taffard[23], F.Tegenfeldt[49], J.Timmermans[31], L.Tkatchev[16], M.Tobin[23], S.Todorovova[12], B.Tome[22], A.Tonazzo[29], P.Tortosa[50], P.Travnicek[12], D.Treille[8], G.Tristram[7], M.Trochimczuk[52], C.Troncon[28], M-L.Turluer[40], I.A.Tyapkin[16], P.Tyapkin[16], S.Tzamarias[11], V.Uvarov[42], G.Valenti[5], P.Van Dam[31], J.Van Eldik[8], A.Van Lysebetten[2], N.van Remortel[2], I.Van Vulpen[8], G.Vegni[28], F.Veloso[22], W.Venus[37], P.Verdier[27], V.Verzi[38], D.Vilanova[40], L.Vitale[47], V.Vrba[12], H.Wahlen[53], A.J.Washbrook[23], C.Weiser[17], D.Wicke[8], J.Wickens[2], G.Wilkinson[35], M.Winter[9], M.Witek[18], O.Yushchenko[42], A.Zalewska[18], P.Zalewski[52], D.Zavrtanik[43], V.Zhuravlov[16], N.I.Zimin[16], A.Zintchenko[16], M.Zupan[11]

[1]Department of Physics and Astronomy, Iowa State University, Ames IA 50011-3160, USA
[2]Physics Department, Universiteit Antwerpen, Universiteitsplein 1, B-2610 Antwerpen, Belgium
and IIHE, ULB-VUB, Pleinlaan 2, B-1050 Brussels, Belgium
and Faculté des Sciences, Univ. de l'Etat Mons, Av. Maistriau 19, B-7000 Mons, Belgium
[3]Physics Laboratory, University of Athens, Solonos Str. 104, GR-10680 Athens, Greece
[4]Department of Physics, University of Bergen, Allégaten 55, NO-5007 Bergen, Norway
[5]Dipartimento di Fisica, Università di Bologna and INFN, Via Irnerio 46, IT-40126 Bologna, Italy
[6]Centro Brasileiro de Pesquisas Físicas, rua Xavier Sigaud 150, BR-22290 Rio de Janeiro, Brazil
and Depto. de Física, Pont. Univ. Católica, C.P. 38071 BR-22453 Rio de Janeiro, Brazil
and Inst. de Física, Univ. Estadual do Rio de Janeiro, rua São Francisco Xavier 524, Rio de Janeiro, Brazil
[7]Collège de France, Lab. de Physique Corpusculaire, IN2P3-CNRS, FR-75231 Paris Cedex 05, France
[8]CERN, CH-1211 Geneva 23, Switzerland
[9]Institut de Recherches Subatomiques, IN2P3 - CNRS/ULP - BP20, FR-67037 Strasbourg Cedex, France
[10]Now at DESY-Zeuthen, Platanenallee 6, D-15735 Zeuthen, Germany
[11]Institute of Nuclear Physics, N.C.S.R. Demokritos, P.O. Box 60228, GR-15310 Athens, Greece
[12]FZU, Inst. of Phys. of the C.A.S. High Energy Physics Division, Na Slovance 2, CZ-180 40, Praha 8, Czech Republic
[13]Dipartimento di Fisica, Università di Genova and INFN, Via Dodecaneso 33, IT-16146 Genova, Italy
[14]Institut des Sciences Nucléaires, IN2P3-CNRS, Université de Grenoble 1, FR-38026 Grenoble Cedex, France
[15]Helsinki Institute of Physics, P.O. Box 64, FIN-00014 University of Helsinki, Finland
[16]Joint Institute for Nuclear Research, Dubna, Head Post Office, P.O. Box 79, RU-101 000 Moscow, Russian Federation
[17]Institut für Experimentelle Kernphysik, Universität Karlsruhe, Postfach 6980, DE-76128 Karlsruhe, Germany
[18]Institute of Nuclear Physics,Ul. Kawiory 26a, PL-30055 Krakow, Poland
[19]Faculty of Physics and Nuclear Techniques, University of Mining and Metallurgy, PL-30055 Krakow, Poland
[20]Université de Paris-Sud, Lab. de l'Accélérateur Linéaire, IN2P3-CNRS, Bât. 200, FR-91405 Orsay Cedex, France
[21]School of Physics and Chemistry, University of Lancaster, Lancaster LA1 4YB, UK
[22]LIP, IST, FCUL - Av. Elias Garcia, 14-1^{o}, PT-1000 Lisboa Codex, Portugal
[23]Department of Physics, University of Liverpool, P.O. Box 147, Liverpool L69 3BX, UK
[24]Dept. of Physics and Astronomy, Kelvin Building, University of Glasgow, Glasgow G12 8QQ
[25]LPNHE, IN2P3-CNRS, Univ. Paris VI et VII, Tour 33 (RdC), 4 place Jussieu, FR-75252 Paris Cedex 05, France
[26]Department of Physics, University of Lund, Sölvegatan 14, SE-223 63 Lund, Sweden
[27]Université Claude Bernard de Lyon, IPNL, IN2P3-CNRS, FR-69622 Villeurbanne Cedex, France
[28]Dipartimento di Fisica, Università di Milano and INFN-MILANO, Via Celoria 16, IT-20133 Milan, Italy
[29]Dipartimento di Fisica, Univ. di Milano-Bicocca and INFN-MILANO, Piazza della Scienza 2, IT-20126 Milan, Italy
[30]IPNP of MFF, Charles Univ., Areal MFF, V Holesovickach 2, CZ-180 00, Praha 8, Czech Republic
[31]NIKHEF, Postbus 41882, NL-1009 DB Amsterdam, The Netherlands
[32]National Technical University, Physics Department, Zografou Campus, GR-15773 Athens, Greece
[33]Physics Department, University of Oslo, Blindern, NO-0316 Oslo, Norway
[34]Dpto. Fisica, Univ. Oviedo, Avda. Calvo Sotelo s/n, ES-33007 Oviedo, Spain
[35]Department of Physics, University of Oxford, Keble Road, Oxford OX1 3RH, UK
[36]Dipartimento di Fisica, Università di Padova and INFN, Via Marzolo 8, IT-35131 Padua, Italy
[37]Rutherford Appleton Laboratory, Chilton, Didcot OX11 OQX, UK
[38]Dipartimento di Fisica, Università di Roma II and INFN, Tor Vergata, IT-00173 Rome, Italy
[39]Dipartimento di Fisica, Università di Roma III and INFN, Via della Vasca Navale 84, IT-00146 Rome, Italy
[40]DAPNIA/Service de Physique des Particules, CEA-Saclay, FR-91191 Gif-sur-Yvette Cedex, France
[41]Instituto de Fisica de Cantabria (CSIC-UC), Avda. los Castros s/n, ES-39006 Santander, Spain
[42]Inst. for High Energy Physics, Serpukov P.O. Box 35, Protvino, (Moscow Region), Russian Federation
[43]J. Stefan Institute, Jamova 39, SI-1000 Ljubljana, Slovenia and Laboratory for Astroparticle Physics,
Nova Gorica Polytechnic, Kostanjeviska 16a, SI-5000 Nova Gorica, Slovenia,
and Department of Physics, University of Ljubljana, SI-1000 Ljubljana, Slovenia
[44]Fysikum, Stockholm University, Box 6730, SE-113 85 Stockholm, Sweden
[45]Dipartimento di Fisica Sperimentale, Università di Torino and INFN, Via P. Giuria 1, IT-10125 Turin, Italy
[46]INFN,Sezione di Torino, and Dipartimento di Fisica Teorica, Università di Torino, Via P. Giuria 1,
IT-10125 Turin, Italy
[47]Dipartimento di Fisica, Università di Trieste and INFN, Via A. Valerio 2, IT-34127 Trieste, Italy
and Istituto di Fisica, Università di Udine, IT-33100 Udine, Italy
[48]Univ. Federal do Rio de Janeiro, C.P. 68528 Cidade Univ., Ilha do Fundão BR-21945-970 Rio de Janeiro, Brazil
[49]Department of Radiation Sciences, University of Uppsala, P.O. Box 535, SE-751 21 Uppsala, Sweden
[50]IFIC, Valencia-CSIC, and D.F.A.M.N., U. de Valencia, Avda. Dr. Moliner 50, ES-46100 Burjassot (Valencia), Spain
[51]Institut für Hochenergiephysik, Österr. Akad. d. Wissensch., Nikolsdorfergasse 18, AT-1050 Vienna, Austria
[52]Inst. Nuclear Studies and University of Warsaw, Ul. Hoza 69, PL-00681 Warsaw, Poland
[53]Fachbereich Physik, University of Wuppertal, Postfach 100 127, DE-42097 Wuppertal, Germany

1 Introduction

The photon structure function has been measured at PETRA and PEP [1–6] and more recently at TRISTAN [7,8] and LEP [9–18] in the reaction $e^+e^- \to e^+e^-X$, where X is a multihadronic system and when one of the scattered leptons is observed at a large scattering angle (tagging condition) while the other, remaining at a small angle, is undetected (anti-tagging condition). This reaction can be described as a deep inelastic $e\gamma$ scattering (DIS), where γ is an almost real photon. The corresponding cross-section is usually expressed in terms of the photon structure functions $F_2^\gamma(x,Q^2)$ and $F_L(x,Q^2)$:

$$\frac{d\sigma}{dE_{tag}d\cos(\theta_{tag})} = \frac{4\pi\alpha^2 E_{tag}}{Q^4 y}\left[(1+(1-y)^2)F_2^\gamma(x,Q^2) - y^2 F_L(x,Q^2)\right]. \qquad (1)$$

Here, E_{tag} and θ_{tag} are the energy and polar angle of the tagged lepton, $Q^2{=}4E_{tag}E_{beam}\sin^2(\theta_{tag}/2)$ is minus the four-momentum squared for the virtual photon emitted from the tagged electron, P^2 corresponds to the same quantity for the anti-tagged photon, the Bjorken variable $x = Q^2/(Q^2+W^2+P^2)$, $y = 1-(E_{tag}/E_{beam})\cos^2\theta_{tag}$ and W is the $\gamma\gamma^*$ invariant mass. Q^2 and P^2 characterise the virtuality of the photons and the anti-tagging condition ensures that P^2 is much smaller than Q^2. Nevertheless the influence of P^2 is not negligible and should be taken into account in the final result. Due to the small values of y in the experimentally accessible region, the influence of F_L on the cross-section is small (from a few to ten percent) and may be taken into account in a simplified way giving an additional uncertainty to these measurements.

The contributions to the photon structure function mostly come from the diagrams in Fig. 1. The point-like contribution (Fig. 1a) can be calculated from QCD. The

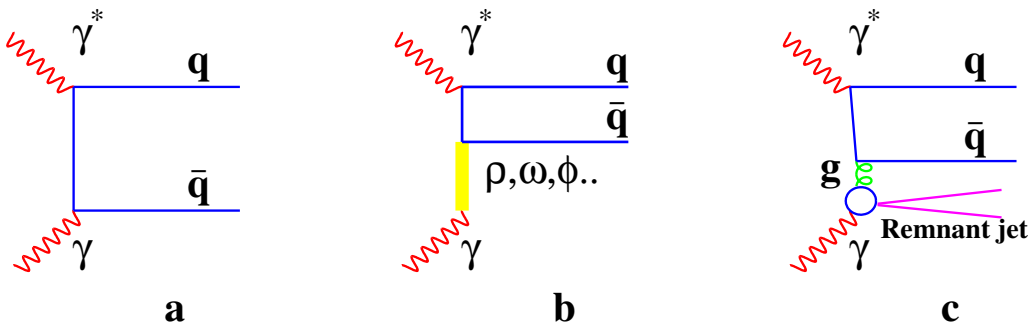

Figure 1: *Contributions to F_2^γ: (a) the point-like, (b) the hadron-like and (c) the Resolved Photon Contribution.*

contribution from the non-perturbative VDM-like component (Fig. 1b) is significant but can not be calculated from perturbation theory. In 1996 OPAL [19] and DELPHI [20] stressed the importance of a proper description of the hadronic state by models used in the analysis. It has been shown by DELPHI [20] that a poor description of the hadronic system produced in $\gamma\gamma^*$ interactions can be due to a missing component in the model. Moreover, problems in the description of the hadronic system lead to a distortion in the correlation between $x_{visible}$ and x_{true} (the measured and true values of x) given by the model. Both factors mentioned above can result in a significant bias in the estimation of the structure function. All studies before 1996 were based on event generators with two

components: a QPM-like model describing the perturbative part (Fig. 1a), and a VDM-like model for the hadron-like part (Fig. 1b). As shown by the DELPHI collaboration in [20], this approach gives a poor description of the final state and, as a result, leads to a significant bias in the structure function estimation. The solution proposed [20] consists of introducing the hard scattering process (Fig. 1c) in the description of the process (the RPC, Resolved Photon Contribution).

Here different partonic densities of the photon can be used to describe the interaction between a highly virtual photon and one of the partons of the resolved photon. Such a modification significantly improves the agreement of simulated events with experimental data. This leads to a more correct description of the final state topology which is crucial for the interpretation of the results. This approach can be realised by making use of the TWOGAM [21] and PHOJET [22] generators. Recently, the general-purpose generators PYTHIA [23] and HERWIG [24] have begun to give reasonable descriptions of DIS. All these new generators use the parton density functions of the photon which are obtained under recent theoretical assumptions [25–31] but require additional input data, namely, experimental measurements of the photon structure function. The influence of the parton density functions on the results given by TWOGAM and PHOJET is much smaller because these generators use it only for the RPC. From this point of view, new measurements will definitely affect the theoretical predictions. Several authors [26,27,32–34] tried to calculate the corresponding F_2^γ but the difference in their results, originating from the treatment of the hadronic part and the choice of boundary conditions for the perturbative equations, is rather large. Hence new studies are needed to improve the understanding of the real photon which will be increasingly important in $\gamma\gamma$ and γp interactions at higher energies.

2 Event selection

A detailed description of the DELPHI detector can be found in [35].

The most important parts of the setup for two-photon physics are the detectors for observing charged particle tracks in the hadronic final state. These tracks are measured in the 1.2 T magnetic field parallel to the beam axis by three cylindrical tracking chambers: the Inner Detector, covering polar angles from 30° to 150° at radii 12 to 28 cm, The Time Projection Chamber, the main tracking device, covering polar angles from 20° to 160° at radii 35 to 111 cm and the Outer Detector covering polar angles from 43° to 137° at radii between 198 and 206 cm. Using the these detectors the momentum resolution is $\sigma(p)/p \approx 0.0015p$ where p is in GeV/c. Tracking in the forward (11-35°) and backward (147-169°) regions is performed by two pairs of Forward Chambers in the end-caps.

In this analysis all the calorimeters are used for event reconstruction thus strengthening the correlation between x_{true} and $x_{visible}$. Electromagnetic energy is measured in the barrel region by the High density Projection Chamber and in the forward-backward regions by the Forward Electro-Magnetic Calorimeter (FEMC) covering the polar angular regions from 10° to 36.5° and 143.5° to 170°.

Hadron shower energies are measured by combining the measurements from the Hadron Calorimeter covering polar angles from 10° to 170°, and from the electromagnetic calorimeters. The luminosity calorimeter STIC (Small angle Tile Calorimeter) is used to measure the energy deposited at small angles (2°-10°). Calorimetric clusters were accepted if their energy deposition exceeded 0.5 GeV in the forward or barrel electromagnetic calorimeters, 1.0 GeV in the hadron calorimeter and 1.5 GeV in the STIC luminometer.

The tagged particles were detected by the luminometer, STIC, and by FEMC.

The data used in this analysis were collected with the DELPHI detector at the LEP e^+e^- collider during the 1994-2000 runs. Samples of 78 pb^{-1} were collected at LEP1 with centre-of-mass energies in the range from 86 GeV to 94 GeV and of 548 pb^{-1} at LEP2 in the energy range 188 GeV to 208 GeV.

The following criteria were used to select a pure sample of $\gamma\gamma^*$ events:

1. The energy deposited by the tagged electron (or positron) must be greater than $0.4 * E_{beam}$ (tagging requirement);
2. No additional clusters with energy exceeding $0.3 * E_{beam}$ may be observed anywhere in the forward calorimeters (anti-tagging requirement);
3. The charged particle multiplicity is 3 or more for the STIC sample and 4 or more in the case of FEMC. This includes only tracks of particles with momenta greater than 0.25 GeV/c with a polar angle between 20° and 160° and an impact parameter less than 4 cm in the radial direction and less than 8 cm along the beam (hadronic final state selection); the tagging particle is not included in the track counting and invariant mass calculation;
4. The visible invariant mass of the hadronic system must be greater than 2.5 GeV/c^2; An upper limit of 25 GeV/c^2 is applied only to the LEP1 data;
5. The vector sum of the transverse momenta of all particles, including the tagged particle, normalised to E_{beam} must be less than 0.12;
6. The absolute value of the total longitudinal momenta of all particles, including the tagged particle, normalised to E_{beam} must be greater than 0.6.

The visible cross-sections for the selected samples and corresponding background cross-sections are presented in Table 1. The cross-sections for the Monte Carlo samples are also presented.

	Background estimates				Experimental signal	Simulation signal		
	σ_{z^0}	$\sigma_{\tau\tau}$	σ_{ee}	$\sigma_{\gamma\gamma}$	$\sigma_{data} - \sigma_{background}$	σ_{TG}	σ_{PH}	σ_{PY}
LEP1 STIC	2.2	1.3	0.4	0.1	38.1±0.7	41.5	27.7	23.2
LEP2 STIC	0.5	1.8	0.6	0.9	41.1±0.3	53.9	45.8	34.8
LEP2 FEMC	0.25	0.05	0	0	0.87±0.04	0.82	1.34	0.88

Table 1. *Estimations of the visible cross-section (pb) of background processes ($e^+e^- \to z\gamma$, $e^+e^- \to \gamma\gamma^* \to \tau^+\tau^-$, $e^+e^- \to \gamma\gamma^* \to e^+e^-$ and $e^+e^- \to \gamma\gamma \to$ hadrons), experimental $\gamma\gamma^*$ signal (with statistical errors) and the signal predictions of the TWOGAM (TG), PHOJET (PH) and PYTHIA (PY) generators.*

The background from $\gamma\gamma^* \to \tau\tau$ and $\gamma\gamma^* \to e^+e^-$ interactions was estimated from simulation as was the background from $Z^0\gamma$ hadronic decays. The interaction $\gamma\gamma \to$ *hadrons* with high energy decay products can produce clusters in the STIC above the tagging threshold and mimic the tagging particle. This contribution is also estimated from simulation. The contamination from other sources of background was found to be much lower. These samples were used as a basis of all studies; some variations of the selection criteria were tried to study the systematics.

The trigger efficiency was studied and found to be $98 \pm 1\%$.

3 Event Generators

Three generators were used to produce simulated samples.

The two-photon event generator TWOGAM [21] (version 2.04) was successfully tested in previous DELPHI studies. The total cross-section is described by the sum of three parts: the point-like (QPM) component, the resolved photon contribution (RPC) and the soft hadronic (VDM) component.

The QPM part is based on the exact decomposition of the matrix element of the process and the exact differential cross-sections [36]. The quark masses are taken to be 0.3 GeV/c^2 for u and d quarks, 0.5 GeV/c^2 for s and 1.6 GeV/c^2 for c quarks.

For the RPC perturbative part the lowest order cross-sections are used. Only the transverse-transverse part of the luminosity function is used in this case. There is no initial or final state parton showering. Strings are formed following the colour flow of the sub-processes. The remnant of a quark is an antiquark (and vice versa), and the remnant of a gluon is a $q\bar{q}$ pair. The program is interfaced to PDFLIB [37], and thus can use any leading order parton density parameterization for the photon. The Gordon-Storrow [33] parton density function set 2 is used in this study. The kinematics of the partonic system is exact for any photon virtuality. This allows for a smooth suppression of the parton densities of resolved photons as their virtuality increases, according to a theoretically motivated ansatz. A transverse momentum cutoff, p_t^{cut}=1.8 GeV/c, is applied to the partons of the resolved photons to separate soft from hard processes.

In this analysis the GVDM [38,39] structure function multiplied by the factor (1-x_{true}) for the soft hadronic part is used. The multihadronic final state is generated as a $q\bar{q}$ pair according to a quark $d\sigma/dp_t^2 \sim exp(-5p_t^2)$ distribution in the $\gamma\gamma$ centre-of-mass system and fragmented using JETSET with σ_q=450MeV/c (the width of Gaussian transverse momenta distribution for primary hadrons) [3].

TWOGAM treats the kinematics of the scattered electron and positron exactly and uses exact (unfactorised) expressions for the two photon luminosity function.

The second Monte Carlo event generator used is PHOJET [22] (version 1.12). The generator includes the exact photon flux simulation for photon-photon processes in lepton-lepton collisions. The ideas and methods used in the program are based mainly on the Dual Parton Model (DPM) [40]. In order to combine the DPM which describes soft processes with the predictive power of perturbative QCD, the event generator is formulated as a two-component model (soft and hard components). On the basis of the optical theorem, Regge phenomenology is used to parametrise the total and elastic cross-sections as well as a series of partial inelastic cross-sections. In order to conserve s-channel unitarity, Gribov's Reggeon calculus is applied [41]. Consequently, the model predicts so-called "multiple parton interactions" in one event. Thus, multiple soft and hard interactions may be generated simultaneously because the unitarization of soft and hard processes is treated in a unified way. Hard scattering processes are simulated using lowest-order perturbative QCD. Initial state and final state parton showers are generated in the leading-log approximation. Some coherence effects (angular ordering in the emissions) are taken into account. For the fragmentation of parton configurations, the JETSET 7.4 program is also used. The GRV [26] parameterisation is used in this analysis. A transverse momentum cutoff, p_t^{cut}=2.5 GeV/c, is applied to the partons of the resolved photons to separate soft from hard processes. The program can run only in the hadronic invariant mass region above 5 GeV/c^2.

The third Monte Carlo program used in this analysis is the PYTHIA (version 6.143) general purpose event generator. Version 6.143 has been used in preference to more recent versions because it represents these DIS data. In this model different kinds of events are distinguished as: direct events, VDM events and anomalous events [25]. In order that the above classification is smooth and free of double counting, the cutoff parameters are

introduced at the level of the real photon fluctuation $\gamma \to q\bar{q}$ and the final hadronic system creation $\gamma\gamma^* \to q\bar{q}$. The VDM and anomalous events together are called resolved ones. These two classes differ in the structure of the underlying event and in the appearance of soft events. The superposition of events mentioned above applies separately for each of the two incoming photons and forms six distinct classes of events: direct-direct, VDM-VDM, anomalous-anomalous, direct-VDM, direct-anomalous and VDM-anomalous. In the case of DIS, only one of the photons is resolved and hence only direct-direct, direct-VDM and direct-anomalous components are used in the model. These three contributions are similar to the TWOGAM and PHOJET classifications.

All generated samples were processed by the full detector simulation and reconstruction programs [35].

4 Comparison of experimental and simulated data

As was mentioned in Section 1, good modelling is necessary for accurate measurements of F_2^γ. Due to finite detector resolution and acceptance, the event final state topology affects the correlation between x_{true} and $x_{visible}$ and the acceptance factor which determines the transition from the x_{true} distribution to F_2^γ. Each component of the model has a different x_{true}-$x_{visible}$ correlation and acceptance factor. Therefore, not only the final state topology for each component but also the cross-section of each component should be properly simulated. To check available models, the inclusive and global event distributions for data should be compared with Monte Carlo predictions with special attention paid to the distributions which are not strongly dependent on x_{true} and cannot be corrected by tuning F_2^γ.

All three generators mentioned above were used to describe the experimental distributions. Table 1 shows that PYTHIA gives a low cross-section for the LEP1 data. Hence only TWOGAM and PHOJET have been used for the LEP1 analysis. The Q^2, E_{tag}/E_{beam} and $W_{visible}$ spectra are shown in Fig. 2 where it can be seen that TWOGAM overestimates and PHOJET underestimates the total visible cross-section. The main difference in TWOGAM comes in the low W region while PHOJET is suppressed in a wide W region. A detailed analysis of these models shows that they differ mostly in their point-like part due to the $p_t = 2.5$ GeV/c cut applied in PHOJET to partons in the final state. As examples of the distributions weakly dependent on x_{true}, spectra of E_{tot} (the total hadronic energy) and N_{trk} (the number of detected charged particles) are shown in Fig. 3(a-b). The distributions reflecting the final state topology are shown in Fig. 3c and Fig. 4. The transverse component of a particle energy out of tag particle plane[1] is one of such distributions (Fig. 3c). The energy flow versus pseudo-rapidity is shown in different Q^2 bins (Fig. 4). The pseudo-rapidity, η, is $-\ln(\tan(\theta/2))$ where θ is the polar angle of final state particles, defined with respect to the beam direction in the hemisphere of the tagged electron. The observed electron is always at negative pseudo-rapidity and is not shown. A reasonable agreement between data and the TWOGAM Monte Carlo prediction is found in all Q^2 ranges. Finally, $x_{visible}$ distributions for the same Q^2 ranges are shown in Fig. 5. From Figs. 2-5 we can conclude that TWOGAM gives the better agreement with the data. The PHOJET and PYTHIA generators with GRV and SaS [27] parameterisations fail to reproduce the data in this Q^2 region, and give a rather poor description of variables defined by the event topology. Hence they are not used in this analysis.

[1] defined as $\sqrt{p_p^2 + m^2}$; p_p is the momentum perpendicular to the plane of the tagged particle and the beam and m is taken as a pion mass.

For the LEP2 data, agreement between PHOJET and PYTHIA simulations and real data becomes better and all three generators mentioned above were used to describe experimental distributions. The Q^2, E_{tag}/E_{beam} and $W_{visible}$ spectra are shown in Fig. 6 for the STIC tagged data. In this kinematic region PHOJET gives the best description of the experimental data whereas TWOGAM overestimates and PYTHIA underestimates the total visible cross-section. The observed x distributions in different Q^2 regions are shown in Fig. 7. Here again PHOJET has the best agreement with data in the low Q^2 region. In the higher Q^2 regions PHOJET overestimates the data. This is a clear indication of wrong Q^2 dependence in this generator, while the behaviour of the predictions of the other generators are similar in all Q^2 regions. The energy flow as a function of the pseudo-rapidity is shown in Fig. 8. All models used in this analysis (especially PHOJET and PYTHIA) fail to describe the energy flow in the central region. This indicates some inconsistency in the description of the final state topology and increases the uncertainty in the extracted F_2^γ.

The Q^2, E_{tag}/E_{beam} and $W_{visible}$ spectra for the sample of events with FEMC tagging are shown in Fig. 9. TWOGAM and PYTHIA give a reasonable description of the experimental data. The wrong Q^2 dependence in PHOJET leads to a significant overestimate of the visible cross-section. The observed x distribution is shown in Fig. 10. The experimental x distribution is well reproduced by TWOGAM and PYTHIA. Such an agreement means a good modelling of the point-like component (dominating in this Q^2 region) by those generators. The energy flow distribution is shown in Fig. 11. It has always been observed that PHOJET version 1.12 has a slightly wrong Q^2 dependence. This is not very important in the low Q^2 region and can be corrected but extrapolation to high Q^2 (FEMC tagging) leads to a serious excess in the PHOJET predictions. Later in this paper only TWOGAM and PYTHIA will be used for the extraction of the structure function in the high Q^2 region.

5 Extraction of the structure function

In the past, F_2^γ has been extracted from data using the method of regularized unfolding (for example, Blobel's unfolding program [42]). In this method a Monte Carlo simulation is used to find a response matrix for the transition from x_{true} to $x_{visible}$ which includes the effect of limited detector acceptance ($W_{visible}$ is lower than W_{true}). Using this matrix, a regularized unfolding derives the x_{true} distribution from the data. As a last step, F_2^γ is determined by reweighting the input structure function of the Monte Carlo according to the ratio of the unfolded x_{true} distribution to the x_{true} in the Monte Carlo. This step takes into account the efficiency because not all events are detected, triggered and pass the selection criteria. Thus, the unfolding method does not take into account differences in the correlations for each of the components in the model. The reweighting factor is also determined by unfolding for a sum of the components in the model without taking into account their differences. These two factors make the usual unfolding procedure inadequate for the task. A priori, some of the components can be correctly simulated in the generator but some should be fitted to the data. Only on the basis of statistical comparisons of many reweighted simulated and experimental distributions can it be decided which components should be modified.

In this analysis the MINUIT program is used. Correction factors A_{ij} are introduced for each of the four bins of the x^i_{true} Monte Carlo distribution (i runs from 1 to 4) and each model component (the QPM j=1, VDM j=2 and RPC j=3). These A_{ij} are the free parameters for the MINUIT fit of the $x_{visible}$ Monte Carlo distribution to the data.

In each fit only four correction factors A_{1k}, A_{2l}, A_{3m} and A_{4n} (where k,l,m,n can be any of 1, 2 or 3) are used. Thus, a total of $3^4 = 81$ combinations are considered in the analysis of the four x_{true} bins. As a result, we have a set of structure functions extracted from the data with corresponding reweighted simulated distributions. Many of the fits give statistically acceptable quality (Fig. 12a) and only on the basis of the analysis of additional distributions (Fig. 12b) can a choice be made between these fits. The statistical analysis of these distributions gives χ^2, which is then considered as a weight factor for the F_2^γ measurement in each fit (Fig. 13).

The difference in each x bin for different fits (Fig. 13) represents the systematic error due to the choice of the model component or combinations of the model components for the fit. Even the statistical error for each x bin depends on the choice of the model due to different efficiencies of event selection for each model. Thus, only a combination of all fits gives the final result.

A test of the fitting procedure has been made. The sample simulated by the PHOJET program was used to extract the structure function used in TWOGAM. The results of this test together with the test of Blobel's unfolding program are shown in Fig. 14(a,b). The curves show the structure function used in TWOGAM. Open circles correspond to the fit with the Monte Carlo sample treated as a sum of three components. The black dots in Fig. 14a better represent the structure function and correspond to the complete MINUIT fitting procedure described above. For comparison, the results of the unfolding procedure are presented in Fig. 14b. As expected, the unfolding procedure leads to some bias and underestimates the errors.

The value of F_L^γ was estimated by TWOGAM and then subtracted from the result. The same generator has been used to estimate correction factors for each x bin which take into account the non-zero virtuality of the target photon in the experiment. All results are then corrected with these factors to get F_2^γ for P^2=0. Bins in x are chosen to have comparable statistics in each and for correlations between the bins to be not too high. For all Q^2 regions, where possible, the same x bins are used: 0.001-0.02, 0.02-0.1, 0.1-0.3, and 0.3-0.8. The correlation matrix for each of the results presented below was checked. The maximum correlation between bins is found to be below 0.35. Applying Q^2 cuts to the full LEP1 event sample, subsamples with average $< Q^2 >$=5.2 GeV$^2/c^4$, $< Q^2 >$=12.7 GeV$^2/c^4$ and $< Q^2 >$=28.5 GeV$^2/c^4$ have been selected. The structure function estimations for these subsamples are presented in Table 2 and illustrated in Fig. 15 together with the predictions of the SaS and GRV models.

$< Q^2 >$ GeV^2/c^4	x range	$< x >$	F_2^γ/α	Stat. err.	Mod. err.	Det. err.	Back. err.	Tot. Sys. err.	Tot. err.
5.2	0.001-0.02	0.01	0.283	0.011	0.010	0.023	0.005	0.026	0.028
	0.02-0.1	0.05	0.203	0.014	0.023	0.007	0.002	0.024	0.028
	0.1-0.5	0.17	0.212	0.020	0.030	0.013	0.004	0.033	0.039
12.7	0.001-0.02	0.01	0.446	0.015	0.010	0.025	0.005	0.027	0.031
	0.02-0.1	0.06	0.317	0.018	0.008	0.010	0.003	0.013	0.022
	0.1-0.3	0.18	0.286	0.034	0.010	0.010	0.005	0.015	0.037
	0.3-0.8	0.39	0.362	0.015	0.020	0.020	0.006	0.029	0.033
28.5	0.02-0.1	0.06	0.413	0.030	0.030	0.018	0.004	0.035	0.043
	0.1-0.3	0.19	0.346	0.015	0.033	0.008	0.002	0.034	0.037
	0.3-0.8	0.45	0.488	0.037	0.030	0.011	0.006	0.033	0.050

Table 2. *Summary of the F_2^γ measurements for LEP1 in three bins of $< Q^2 >$.*

The first error is the statistical one (Stat. err.) which in this approach also depends on the model and in some sense carries some systematic uncertainty. The model dependent shift in F_2^γ measured in each x bin is interpreted as a modelling systematic (Mod. err.)

and is shown in the Tables 2-5 in the sixth column. The fit shows good agreement between most of distributions in data and Monte Carlo but does not help to improve the agreement in the energy flow distribution. Hence the systematic error due to the uncertainty in the energy flow description was studied separately. As is seen from the Monte Carlo study, a correction to the E_{flow} leads to a shift of the extracted value of F_2^γ. This shift is interpreted as a systematic error (E_{flow}). The shift in the unfolding results due to variations in the selection criteria (for example for W_{min} or N_{min}^{trk}), thresholds for the detection of neutral particles by the calorimeters and the uncertainty in the measurement of invariant mass was interpreted as a detector dependent systematic error (Det. err.). Depending on the calculation method, this error varies by about $\pm 20\%$. The background systematic error (Back. err.) reflects the uncertainty in the knowledge of the background and was estimated from the $Z^0\gamma$ hadronic and $\gamma\gamma \to \tau\tau$ simulations as the uncertainty with which the corresponding data samples can be described. There are certainly some other sources of systematics in the measurements but their influence is estimated to be much smaller.

The LEP2 data were sliced in Q^2 to make subsamples with average $< Q^2 >$ values of 19, 40, and 101 GeV$^2/c^4$. The results of the F_2^γ extraction from the data using TWOGAM (black points), PHOJET (open circles), and PYTHIA (open triangles) are shown in Fig. 16 (also Tables 3-5) together with the TWOGAM, SaS, and GRV model predictions. The maximum correlation between bins here is below 0.40.

Model	x range	$< x >$	F_2^γ/α	Stat. err.	Mod. err.	E_{flow} err.	Det. err.	Back. err.	Tot. Sys. err.	Tot. err.
1	0.001-0.02	0.009	0.490	0.015	0.028	0.022	0.018	0.004	0.040	0.043
2		0.009	0.425	0.013	0.026	0.027	0.018	0.004	0.042	0.044
3		0.009	0.399	0.020	0.038	0.025	0.018	0.004	0.049	0.053
1	0.02-0.1	0.051	0.311	0.010	0.007	0.019	0.010	0.002	0.023	0.025
2		0.049	0.306	0.010	0.005	0.080	0.010	0.002	0.081	0.081
3		0.053	0.334	0.025	0.015	0.040	0.010	0.002	0.044	0.051
1	0.001-0.1	0.044	0.336	0.011	0.025	0.017	0.015	0.003	0.034	0.036
2		0.042	0.321	0.010	0.024	0.070	0.015	0.003	0.075	0.076
3		0.046	0.352	0.024	0.035	0.035	0.015	0.003	0.052	0.057
1	0.1-0.3	0.168	0.328	0.008	0.010	0.017	0.010	0.003	0.022	0.024
2		0.178	0.317	0.010	0.012	0.050	0.010	0.003	0.052	0.054
3		0.174	0.235	0.012	0.020	0.025	0.010	0.003	0.034	0.036
1	0.3-0.8	0.403	0.374	0.028	0.015	0.019	0.013	0.003	0.028	0.039
2	0.3-0.5	0.373	0.309	0.050	0.040	0.060	0.013	0.003	0.073	0.088
3	0.3-0.5	0.390	0.341	0.055	0.065	0.040	0.013	0.003	0.077	0.096

Table 3. *Summary of F_2^γ estimated by the TWOGAM(1), PHOJET(2) and PYTHIA(3) generated data for the sample with average $< Q >^2$=19 GeV$^2/c^4$.*

Model	x range	$< x >$	F_2^γ/α	Stat. err.	Mod. err.	E_{flow} err.	Det. err.	Back. err.	Tot. Sys. err.	Tot. err.
1	0.001-0.02	0.012	0.655	0.010	0.029	0.035	0.023	0.004	0.047	0.048
2		0.012	0.630	0.015	0.020	0.024	0.025	0.004	0.040	0.043
3		0.012	0.610	0.020	0.047	0.045	0.025	0.004	0.069	0.073
1	0.02-0.1	0.055	0.415	0.007	0.022	0.015	0.008	0.002	0.028	0.029
2		0.055	0.384	0.012	0.014	0.048	0.012	0.002	0.051	0.053
3		0.056	0.485	0.015	0.025	0.025	0.012	0.002	0.037	0.040
1	0.001-0.1	0.048	0.441	0.008	0.020	0.018	0.007	0.002	0.028	0.029
2		0.048	0.418	0.012	0.018	0.041	0.010	0.002	0.046	0.048
3		0.049	0.500	0.016	0.035	0.032	0.010	0.002	0.049	0.052
1	0.1-0.3	0.181	0.438	0.022	0.034	0.013	0.012	0.004	0.039	0.044
2		0.177	0.325	0.018	0.020	0.032	0.013	0.004	0.040	0.044
3		0.184	0.290	0.015	0.045	0.030	0.013	0.004	0.056	0.058
1	0.3-0.8	0.430	0.501	0.017	0.020	0.012	0.013	0.005	0.027	0.031
2		0.428	0.590	0.024	0.025	0.080	0.015	0.005	0.085	0.089
3		0.429	0.371	0.022	0.030	0.085	0.015	0.005	0.092	0.094

Table 4. *Summary of F_2^γ estimated by the TWOGAM(1), PHOJET(2) and PYTHIA(3) generated data for the full sample with average $< Q^2 >$=40 GeV$^2/c^4$.*

Model	x range	$< x >$	F_2^γ/α	Stat. err.	Mod. err.	E_{flow} err.	Det. err.	Back. err.	Tot. Sys. err.	Tot. err
1	0.001-0.02	0.013	0.885	0.101	0.106	0.035	0.023	0.005	0.117	0.154
2		0.014	0.939	0.076	0.139	0.024	0.025	0.005	0.143	0.162
3		0.014	0.965	0.065	0.140	0.045	0.025	0.005	0.149	0.163
1	0.02-0.1	0.058	0.530	0.031	0.022	0.015	0.007	0.002	0.028	0.042
2		0.058	0.563	0.020	0.015	0.048	0.010	0.002	0.051	0.055
3		0.061	0.663	0.018	0.025	0.035	0.010	0.002	0.044	0.047
1	0.001-0.1	0.051	0.587	0.032	0.020	0.013	0.006	0.002	0.025	0.041
2		0.051	0.569	0.021	0.018	0.040	0.009	0.002	0.045	0.050
3		0.053	0.668	0.019	0.023	0.033	0.009	0.002	0.041	0.045
1	0.1-0.3	0.190	0.492	0.023	0.015	0.012	0.013	0.004	0.024	0.033
2		0.184	0.326	0.016	0.030	0.032	0.014	0.004	0.046	0.049
3		0.191	0.458	0.015	0.036	0.030	0.014	0.004	0.049	0.051
1	0.3-0.8	0.464	0.648	0.029	0.020	0.012	0.013	0.005	0.027	0.040
2		0.493	0.670	0.030	0.024	0.080	0.015	0.005	0.085	0.090
3		0.464	0.793	0.025	0.030	0.085	0.015	0.005	0.091	0.098

Table 5. *Summary of F_2^γ estimated by the TWOGAM(1), PHOJET(2) and PYTHIA(3) generated data for the sample with average $< Q^2 >$=101 GeV$^2/c^4$.*

The sample selected with FEMC tagging has been used to extract the structure function in the highest Q^2 region available at DELPHI. Only TWOGAM and PYTHIA were used in the analysis for this kinematic region. Results are presented in Fig. 17 and Table 6. The maximum correlation between bins is found to be below 0.20.

Model	x range	$< x >$	F_2^γ/α	Stat. err.	Mod. err.	Det. err.	Back. err.	Tot. Sys. err.	Tot. err.
1	0.01-0.3	0.172	1.011	0.084	0.104	0.148	0.122	0.217	0.231
2		0.161	0.582	0.095	0.154	0.139	0.111	0.235	0.253
1	0.3-0.8	0.520	0.940	0.050	0.077	0.072	0.024	0.108	0.119
2		0.500	0.984	0.055	0.089	0.068	0.020	0.114	0.126

Table 6. *Summary of F_2^γ estimated by the TWOGAM(1) and PYTHIA(2) generated data for the sample with average $< Q^2 >$=700 GeV$^2/c^4$.*

The TWOGAM generator was used to study the Q^2 evolution of F_2^γ from the results in Tables 2-6 for the x intervals 0.001-0.02, 0.001-0.1, 0.1-0.3 and 0.3-0.8. The F_2^γ evolution is shown in Fig. 18 together with results from the other LEP experiments: OPAL [12–14], L3 [16,17] and ALEPH [18]. The function $a + bLog_{10}(Q^2)$ is fitted to the DELPHI data taking into account the total errors. The parameters obtained by the fit are shown in Table 7.

x range	a	b	χ^2/ndf
0.001-0.02	-0.004±0.065	0.402±0.060	0.18
0.001-0.1	0.032±0.039	0.261±0.034	0.28
0.1-0.3	0.049±0.066	0.223±0.043	0.67
0.3-0.8	-0.032±0.071	0.343±0.046	0.37

Table 7. *The Q^2 fit results.*

In all four x intervals the $Log_{10}(Q^2)$ dependence is consistent with a linear function.

6 Conclusions

The photon hadronic structure function, F_2^γ, has been studied in the data taken by the DELPHI detector at LEP. The measurements have been made in the Q^2 interval from 3 to 2600 GeV$^2/c^4$ and in the x range from 0.001 to 0.8. Conclusions drawn from the results in Tables 2-5 are the following:
1. The results for F_2^γ with their total uncertainties are reasonably consistent as extracted from the DELPHI data using three generators;
2. The largest contributions to the overall uncertainty come from the model dependent systematics and problems in the simulation of the event final state topology which can be seen in Figs. 4 and 8. The systematic errors for the results extracted with the use of PHOJET and PYTHIA are larger than the errors using TWOGAM, mostly due to the greater disagreement between data and Monte Carlo predictions given by these generators in the description of the event topology.
3. In all Q^2 regions, the results are higher than the GRV and SaS model predictions and are consistent with the TWOGAM prediction in the lowest x bin. In the x region larger than 0.05, results are systematically lower than the TWOGAM prediction. Results are close to the GRV model in the x region above 0.1.

The Monte Carlo generators giving the best descriptions of the process are used in this analysis.

The hadronic structure function is estimated as a function of x in seven Q^2 intervals, with mean squared momentum transfer $< Q^2 >$=5.2, 12.7, 19, 28.5, 40, 101 and 700 GeV$^2/c^4$. Combining all DELPHI data, the evolution of F_2^γ with Q^2 in the x ranges $0.001 < x < 0.02$, $0.001 < x < 0.1$, $0.1 < x < 0.3$ and $0.3 < x < 0.8$ has been shown. From these results the slope $\alpha^{-1} dF_2^\gamma / dLog_{10}(Q^2)$ is found to be consistent with the logarithmic evolution of F_2^γ with Q^2. The proposed method for the photon structure function study has been demonstrated to be consistent. The model dependent systematic error shown by this procedure is larger than that estimated by the unfolding procedure and better reflects our knowledge of the process. Better modelling based on the improved available data can reduce such an error.

Acknowledgements

We are greatly indebted to our technical collaborators, to the members of the CERN-SL Division for the excellent performance of the LEP collider, and to the funding agencies for their support in building and operating the DELPHI detector.
We acknowledge in particular the support of
Austrian Federal Ministry of Education, Science and Culture, GZ 616.364/2-III/2a/98,
FNRS–FWO, Flanders Institute to encourage scientific and technological research in the industry (IWT), Federal Office for Scientific, Technical and Cultural affairs (OSTC), Belgium,
FINEP, CNPq, CAPES, FUJB and FAPERJ, Brazil,
Czech Ministry of Industry and Trade, GA CR 202/99/1362,
Commission of the European Communities (DG XII),
Direction des Sciences de la Matière, CEA, France,
Bundesministerium für Bildung, Wissenschaft, Forschung und Technologie, Germany,
General Secretariat for Research and Technology, Greece,
National Science Foundation (NWO) and Foundation for Research on Matter (FOM), The Netherlands,
Norwegian Research Council,
State Committee for Scientific Research, Poland, SPUB-M/CERN/PO3/DZ296/2000, SPUB-M/CERN/PO3/DZ297/2000 and 2P03B 104 19 and 2P03B 69 23(2002-2004)
JNICT–Junta Nacional de Investigação Científica e Tecnológica, Portugal,
Vedecka grantova agentura MS SR, Slovakia, Nr. 95/5195/134,
Ministry of Science and Technology of the Republic of Slovenia,
CICYT, Spain, AEN99-0950 and AEN99-0761,
The Swedish Natural Science Research Council,
Particle Physics and Astronomy Research Council, UK,
Department of Energy, USA, DE-FG02-01ER41155,
EEC RTN contract HPRN-CT-00292-2002.

References

[1] PLUTO Collab., Ch. Berger et al., Z.Phys. **C26** (1984) 353;
Phys. Lett. **B149** (1984) 421;
Nucl. Phys. **B281** (1987) 356.
[2] JADE Collab., W. Bartel et al., Z.Phys. **C24** (1984) 231.
[3] TASSO Collab., H. Althoff et. al., Z.Phys. **C31** (1986) 527.
[4] CELLO Coll., H.-J. Behrend et al., Phys. Lett. **B126** (1983) 391.
[5] TPC/2γ Coll., A. Aihara et al., Phys. Rev. Lett. **58** (1987) 97;
TPC/2γ Coll., A. Aihara et al., Phys. Rev. **54** 41 (1985) 736.
[6] TPC/2γ Coll., A. Aihara et al., Z.Phys. **C34** (1987) 1.
[7] AMY Collab., R. Sasaki et al., Phys. Lett. **B252** (1990) 491;
S.K. Sahu et al., Phys. Lett. **B346** (1995) 208.
[8] TOPAZ Collab., K. Muramatsu et al., Phys. Lett. **B332** (1994) 478.
[9] OPAL Collab., R. Akers et al., Z.Phys. **C61** (1994) 199.
[10] DELPHI Coll., P. Abreu et al. Z.Phys. **C69** (1996) 223.
[11] OPAL Coll., K. Ackerstaff et al., Z.Phys. **C74** (1997) 33.
[12] OPAL Coll., K. Ackerstaff et al., Phys. Lett. **B411** (1997) 387.

[13] OPAL Coll., K. Ackerstaff et al., Phys. Lett. **B412** (1997) 225.
[14] OPAL Coll., G. Abbiendi et al., Eur. Phys. J. **C18** (2000) 15.
[15] L3 Coll., M. Acciarri et al., Phys. Lett. **B436** (1998) 403.
[16] L3 Coll., M. Acciarri et al., Phys. Lett. **B447** (1999) 147.
[17] L3 Coll., M. Acciarri et al., Phys. Lett. **B483** (2000) 373.
[18] ALEPH Coll., R. Barate et al., Phys. Lett. **B458** (1999) 152.
[19] OPAL Coll., Jan A. Lauber, Proc. of the 28th Int. Conf on High Energy Physics, World Scientific Publishing Co. Pte. Ltd., (1996) 725.
[20] DELPHI Coll., Igor Tyapkin, Proc. of the 28th Int. Conf on High Energy Physics, World Scientific Publishing Co. Pte. Ltd., (1996) 729.
[21] S. Nova, A. Olshevsky, T. Todorov, DELPHI-90-35 (unpublished).
[22] Humboldt University, D-10099 Berlin, FRG.
[23] T. Sjöstrand, Comp. Phys. Comm. **82** (1994) 74.
[24] G. Marchesini, B.R. Webber, G. Abbiendi, I.G. Knowles, M.H. Seymour and L. Stanco, Computer Phys. Comm. **67** (1992) 465.
[25] Workshop on Physics at LEP2 ,CERN 96-01 v2 (1996).
[26] M. Gluck, E. Reya and A. Vogt, Phys. Rev. **D45** (1992) 3986.
[27] G.A. Schuler and T. Sjostrand, Z. Phys. **C68** (1995) 607.
[28] G.A. Schuler, T. Sjostrand, Phys. Lett. **B300** (1993) 169; Nucl. Phys. **B407** (1993) 539.
[29] G.A. Schuler, T. Sjostrand, in "Two-Photon Physics from DAFNE to LEP200 and Beyond", World Scientific, Singapore, 1994, eds. F. Kapusta and J. Parisi, p163; T Sjostrand, in "XXIV International Symposium on Multiparticle Dynamics 1994", World Scientific, Singapore, 1995, eds. A. Giovannini, S. Lupia and R. Ugoccioni, p221.
[30] G. Marchesini and B.R. Webber, Nucl. Phys. **386** (1992) 215.
[31] M.H. Seymour, Comput. Phys. Commun. **90** (1995) 95.
[32] M. Drees and R.M.Godbole, J. Phys. **G21** (1995) 1559.
[33] L.E. Gordon and J.K. Storrow, Z.Phys. **C56** (1992) 307.
[34] H. Abramovicz, K. Charchula and A. Levy, Phys. Lett. **B269** (1991) 458.
[35] DELPHI Coll., P. Aarnio et al., Nucl. Instr. and Meth., **A303** (1991) 233.
DELPHI Coll., P. Abreu et al., Nucl. Instr. and Meth., **A378** (1996) 57.
[36] V.N. Baier et al., Phys. Rep. **78** (1981) 293.
[37] H. Plothow-Besch, PDFLIB : A Library of all available Parton Density Functions of the Nucleon, the Pion and the Photon and the corresponding α_s calculations, CERN-PPE-92-123.
[38] J.J. Sakurai and D. Schildknecht, Phys. Lett. **B41** (1972) 489; Phys. Lett. **41B** (1972) 489.
[39] I.F. Ginzburg and V.G. Serbo, Phys. Lett., **B109** (1982) 1.
[40] A. Capella, et al., Phys. Rep. **236** (1994) 227.
[41] V.N. Gribov Sov. Phys. JETP 26 (1968) 414; V.N. Gribov and A.A. Migdal Sov. J. Nucl. Phys. 8 (1969) 583.
[42] V. Blobel, Proceedings of the CERN School of Computing, Aiguablava, Spain, (1984), CERN 85-09.

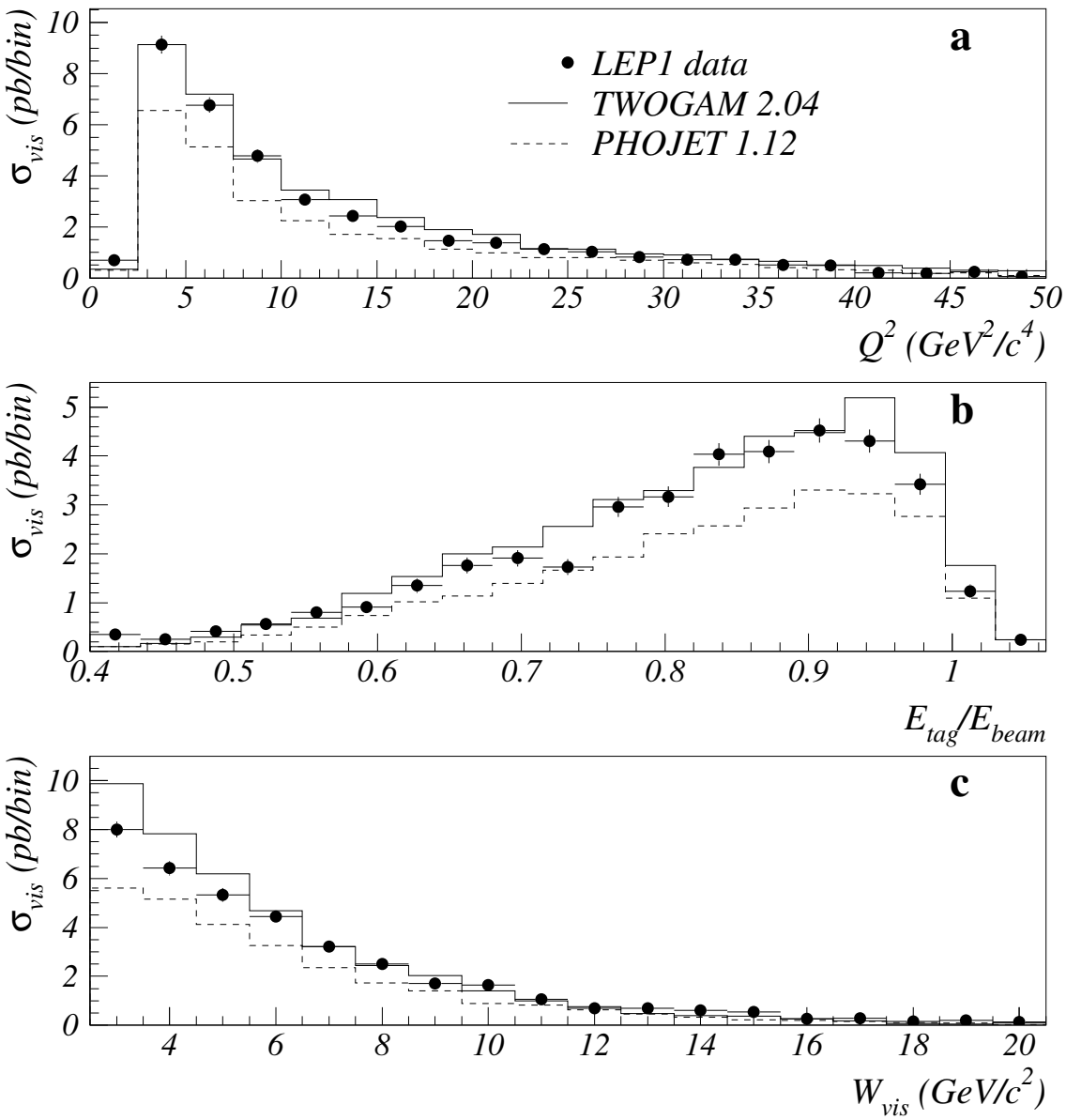

Figure 2: *Comparison between data and Monte Carlo predictions for the full LEP1 sample with* $< Q^2 >$*=12.7 GeV*$^2/c^4$*: a)* Q^2*, b) tagging energy, c) invariant mass. Points are data and the lines show the predictions of TWOGAM (solid line) and PHOJET (dashed line).*

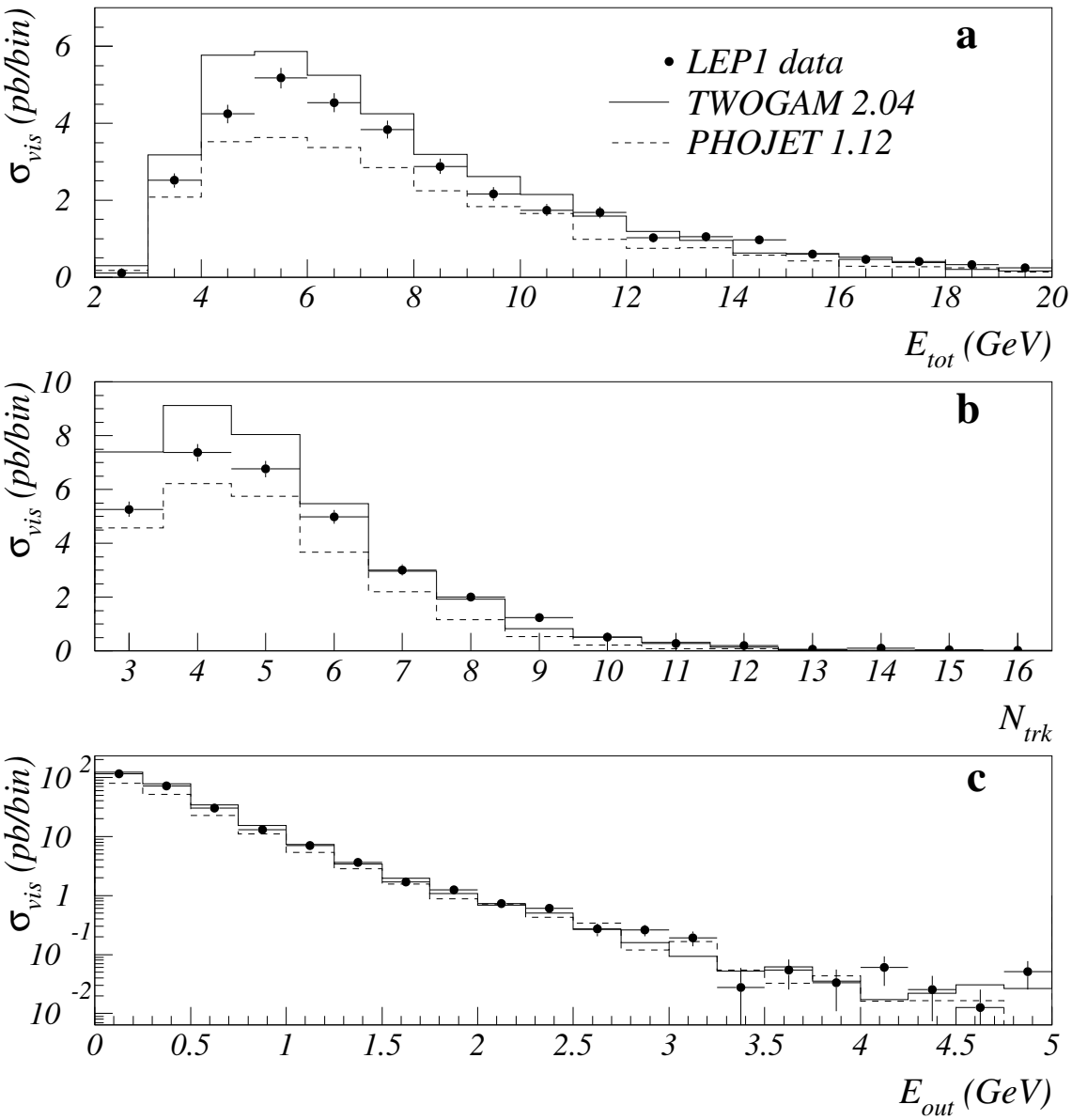

Figure 3: *Comparison between data and Monte Carlo predictions for the full LEP1 sample with* $< Q^2 >$*=12.7 GeV*$^2/c^4$*: a) total energy of the hadronic system, b) total number of charged particles, c) transverse component of the hadronic energy out of the plane of the tagged particle. Points are data and the lines show the predictions of TWOGAM (solid line) and PHOJET (dashed line).*

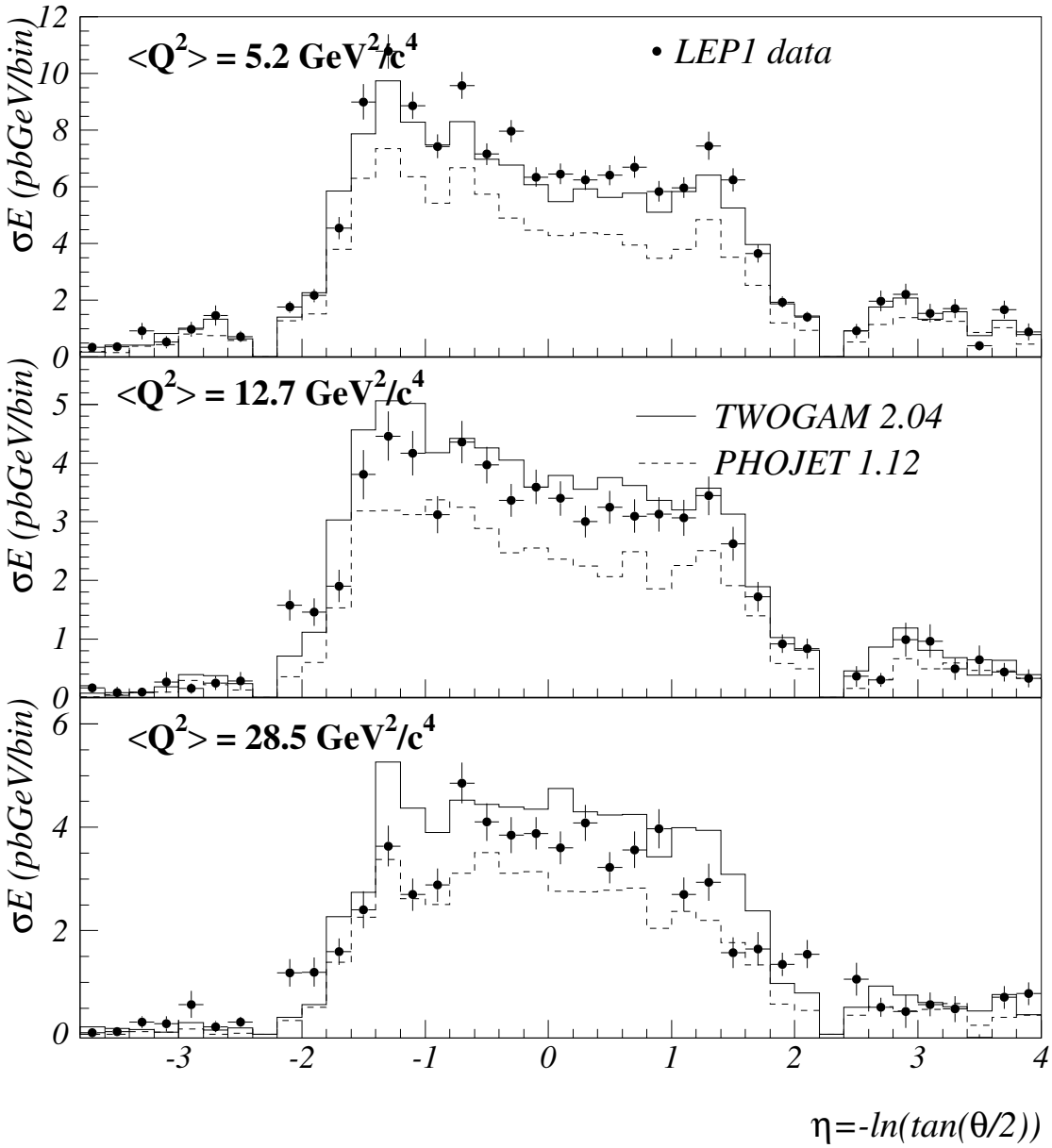

Figure 4: *Comparison of the hadronic energy flow for data and Monte Carlo predictions versus pseudo-rapidity for the LEP1 STIC tagged data in different* $< Q^2 >$ *regions. Points are data and the lines show the predictions of TWOGAM (solid line) and PHOJET (dashed line).*

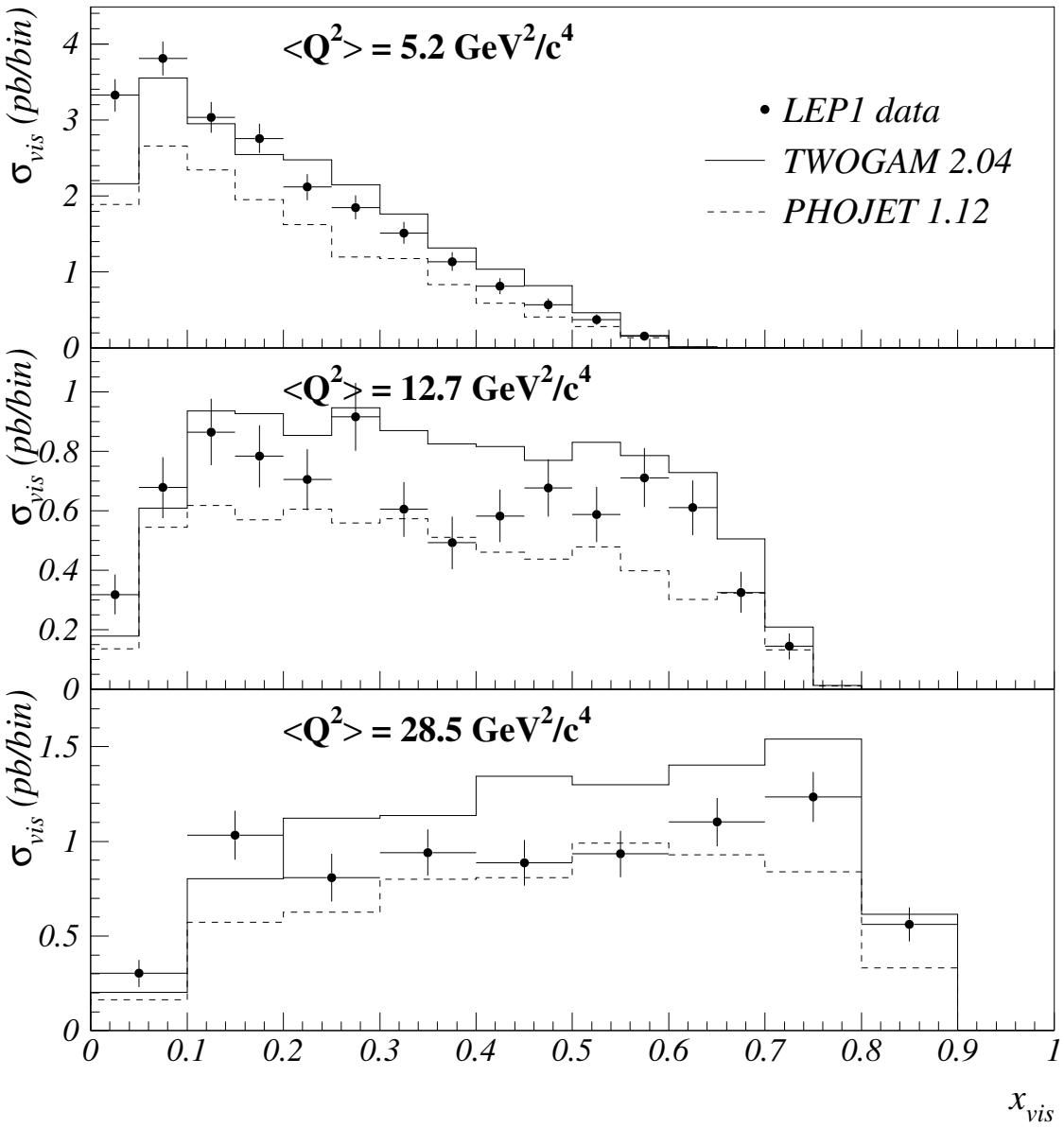

Figure 5: *Comparison between data and Monte Carlo predictions for the LEP1 STIC tagged data in different $< Q^2 >$ regions. Points are data and the lines show the predictions of TWOGAM (solid line), PHOJET (dashed line).*

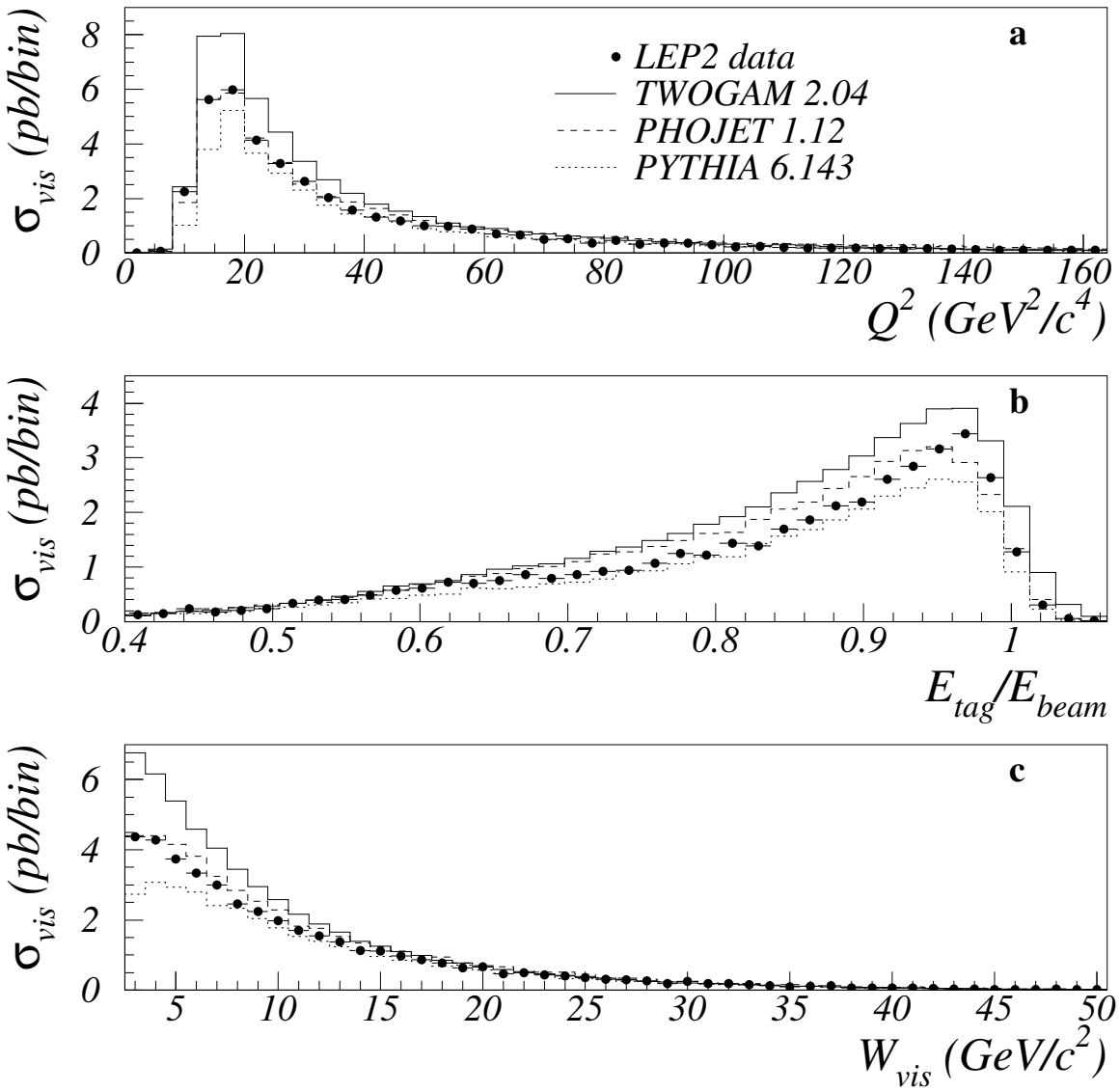

Figure 6: *Comparison between data and Monte Carlo predictions for the LEP2 STIC tagged data: a) Q^2, b) tagging energy, c) invariant mass. Points are data and the lines show the predictions of TWOGAM (solid line), PHOJET (dashed line) and PYTHIA (dotted line).*

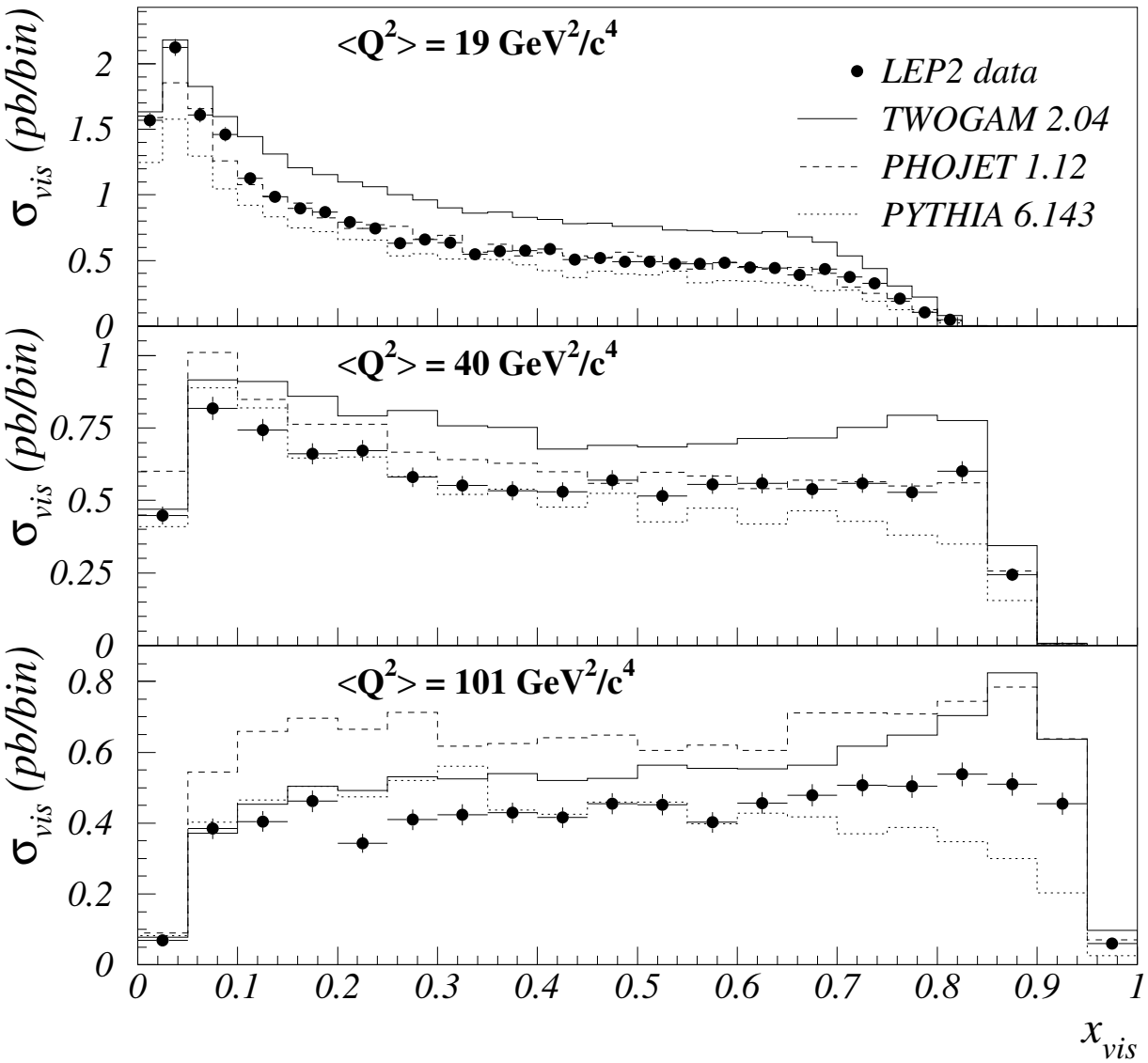

Figure 7: *Comparison between $x_{visible}$ distributions for the data and Monte Carlo predictions for the LEP2 STIC tagged samples in different $< Q^2 >$ regions. Points are data and the lines show the predictions of TWOGAM (solid line), PHOJET (dashed line) and PYTHIA (dotted line).*

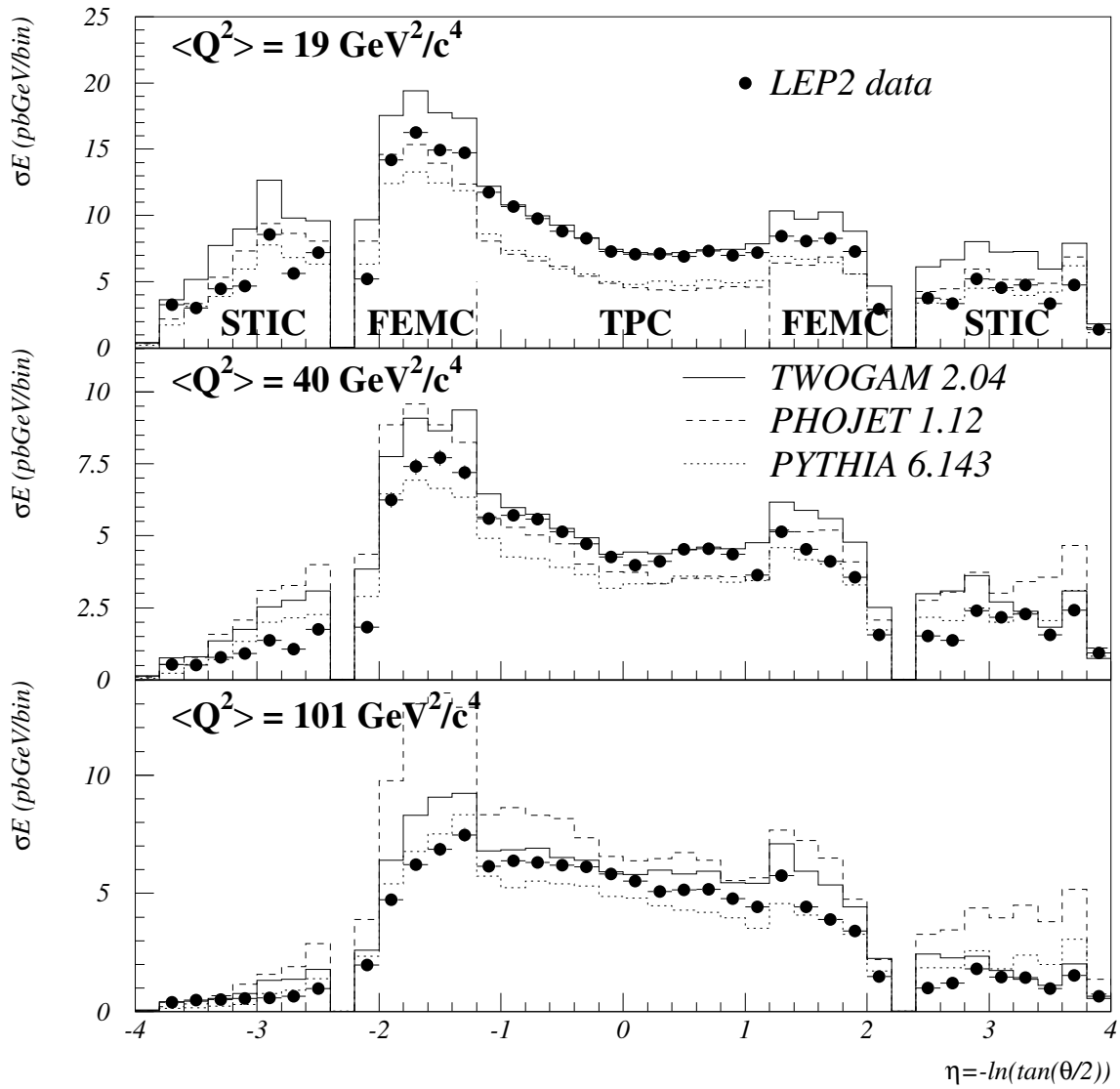

Figure 8: *Comparison of the hadronic energy flow versus pseudo-rapidity for the LEP2 STIC tagged data and Monte Carlo predictions in different $< Q^2 >$ regions. Points are data and the lines show the predictions of TWOGAM (solid line), PHOJET (dashed line) and PYTHIA (dotted line). The main contributing detector components are shown in the upper plot.*

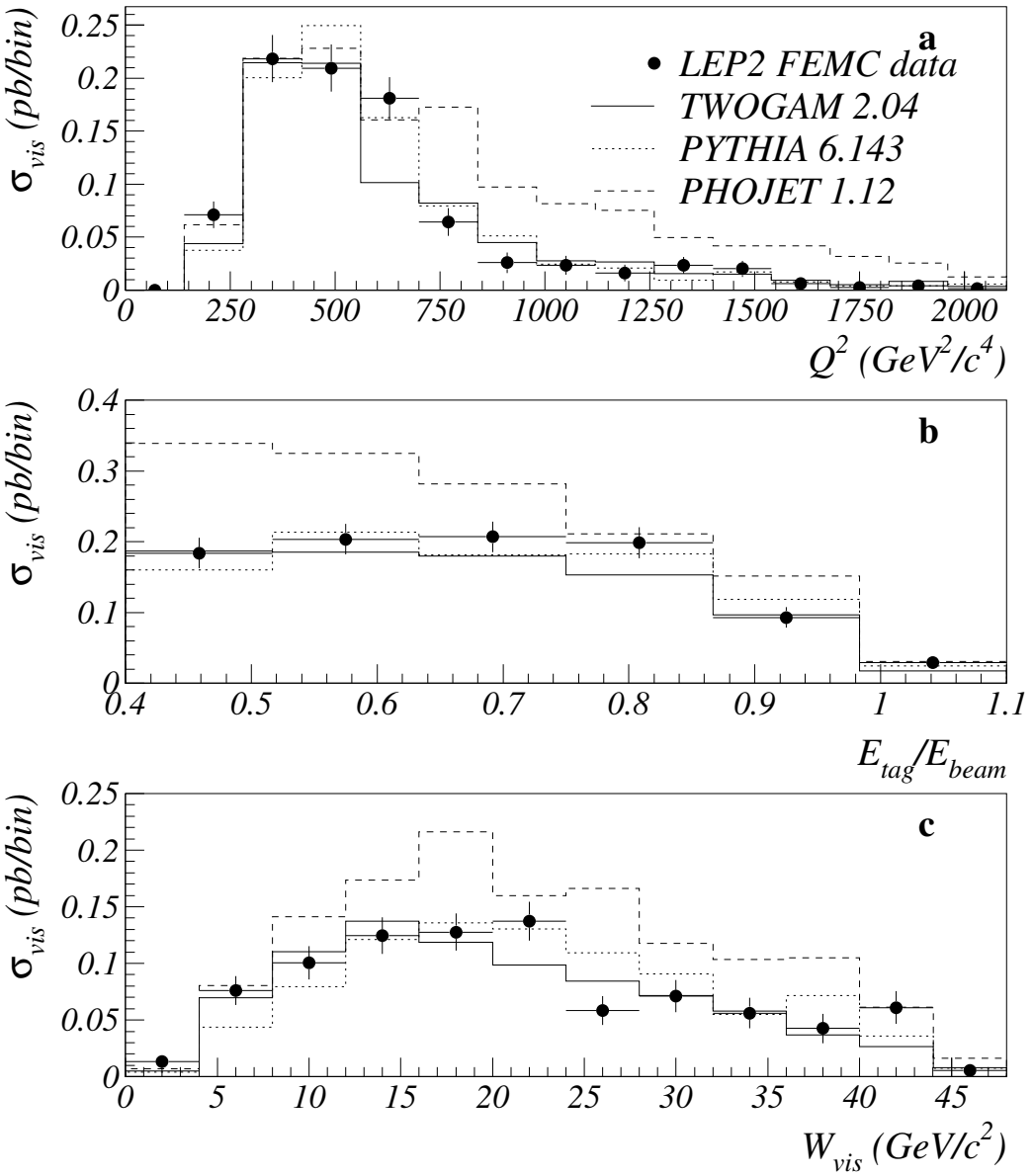

Figure 9: *Comparison between data and Monte Carlo predictions for the LEP2 FEMC tagged sample: a) Q^2, b) tagging energy, c) invariant mass. Points are data and the lines show the predictions of TWOGAM (solid line), PHOJET (dashed line) and PYTHIA (dotted line).*

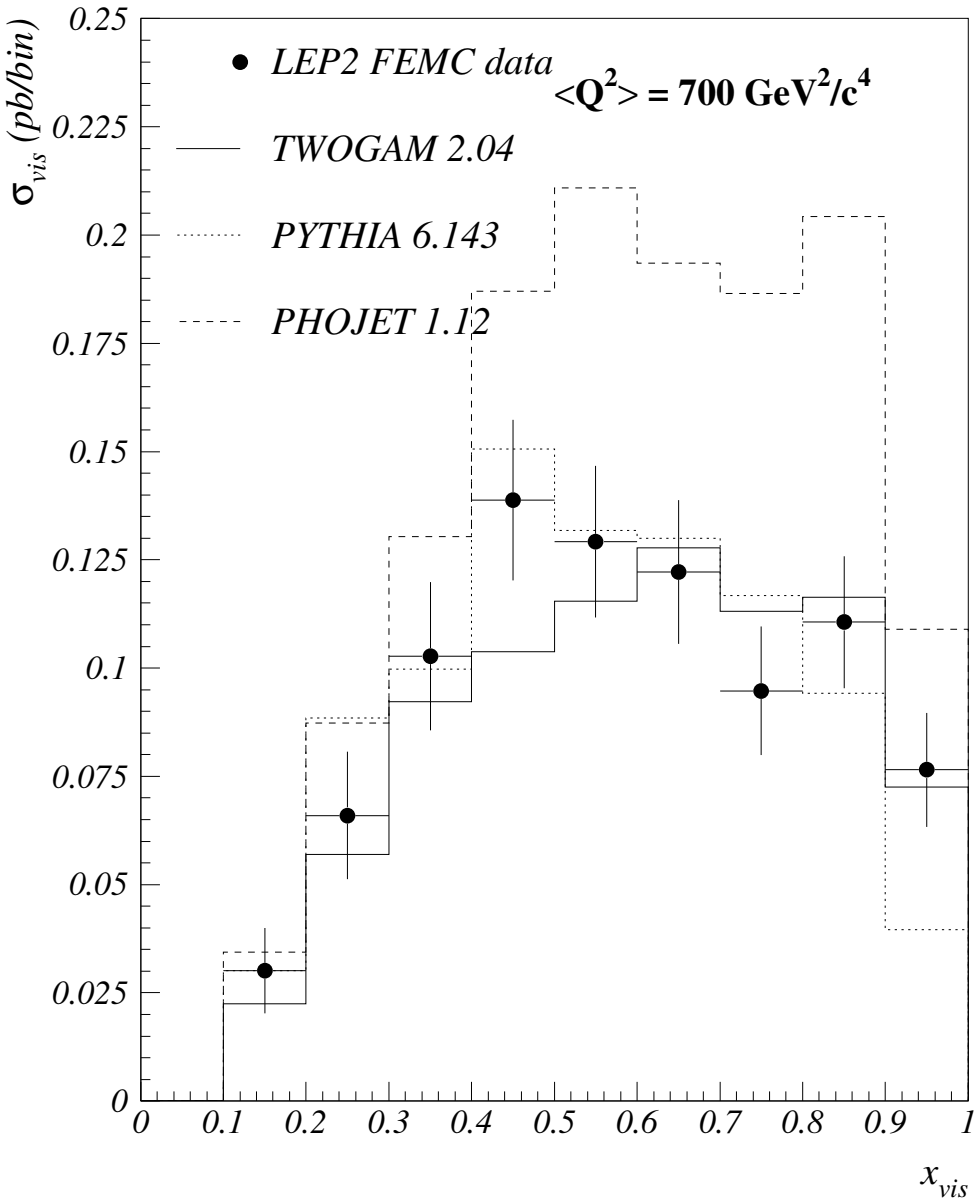

Figure 10: *Comparison between data and Monte Carlo predictions for the LEP2 FEMC tagged sample $x_{visible}$ distribution. Points are data and the lines show the predictions of TWOGAM (solid line), PHOJET (dashed line) and PYTHIA (dotted line).*

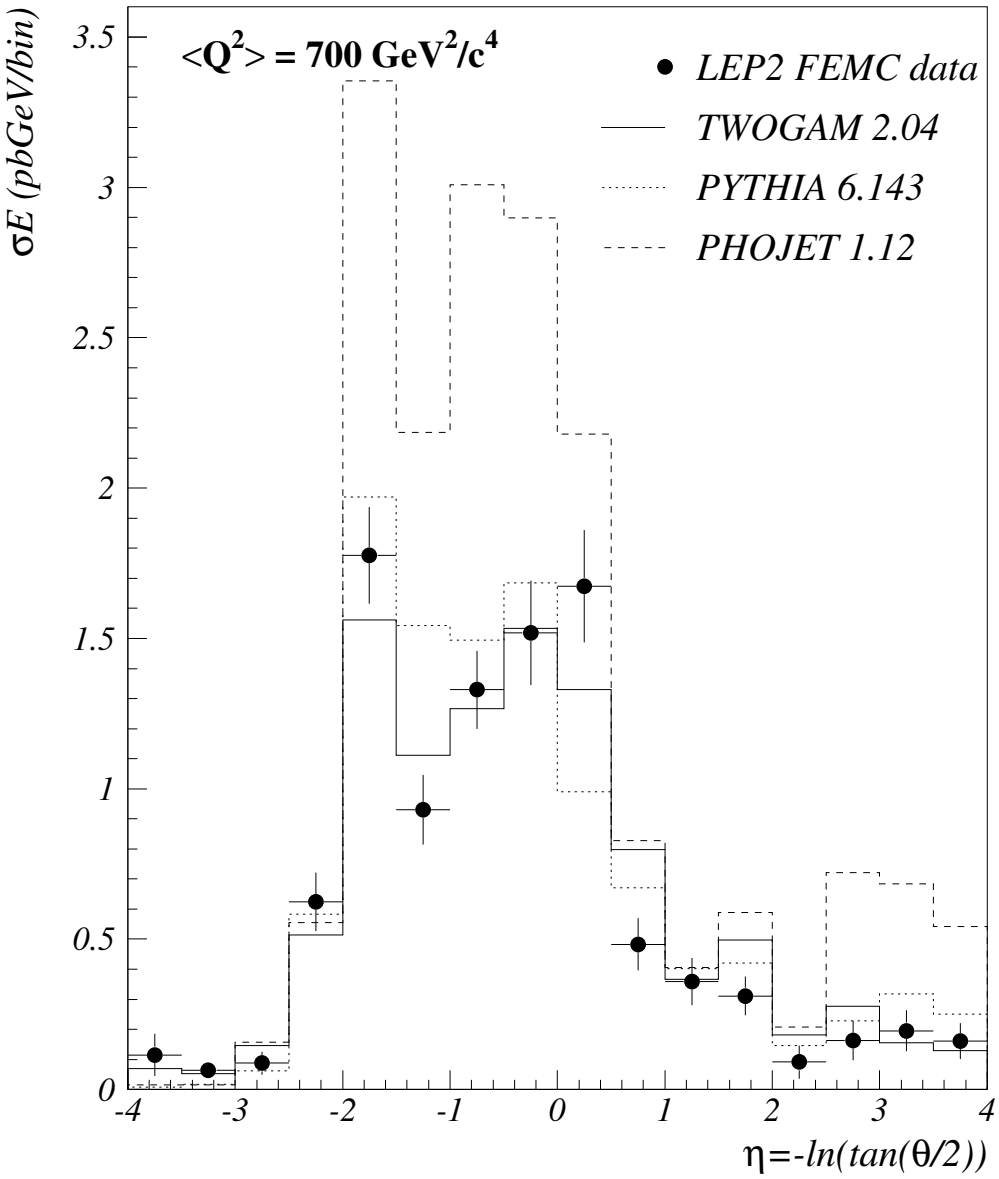

Figure 11: *Comparison of hadronic energy flow for data and Monte Carlo predictions versus pseudo-rapidity for the LEP2 FEMC selected events. Points are data and the lines show the predictions of TWOGAM (solid line), PHOJET (dashed line) and PYTHIA (dotted line).*

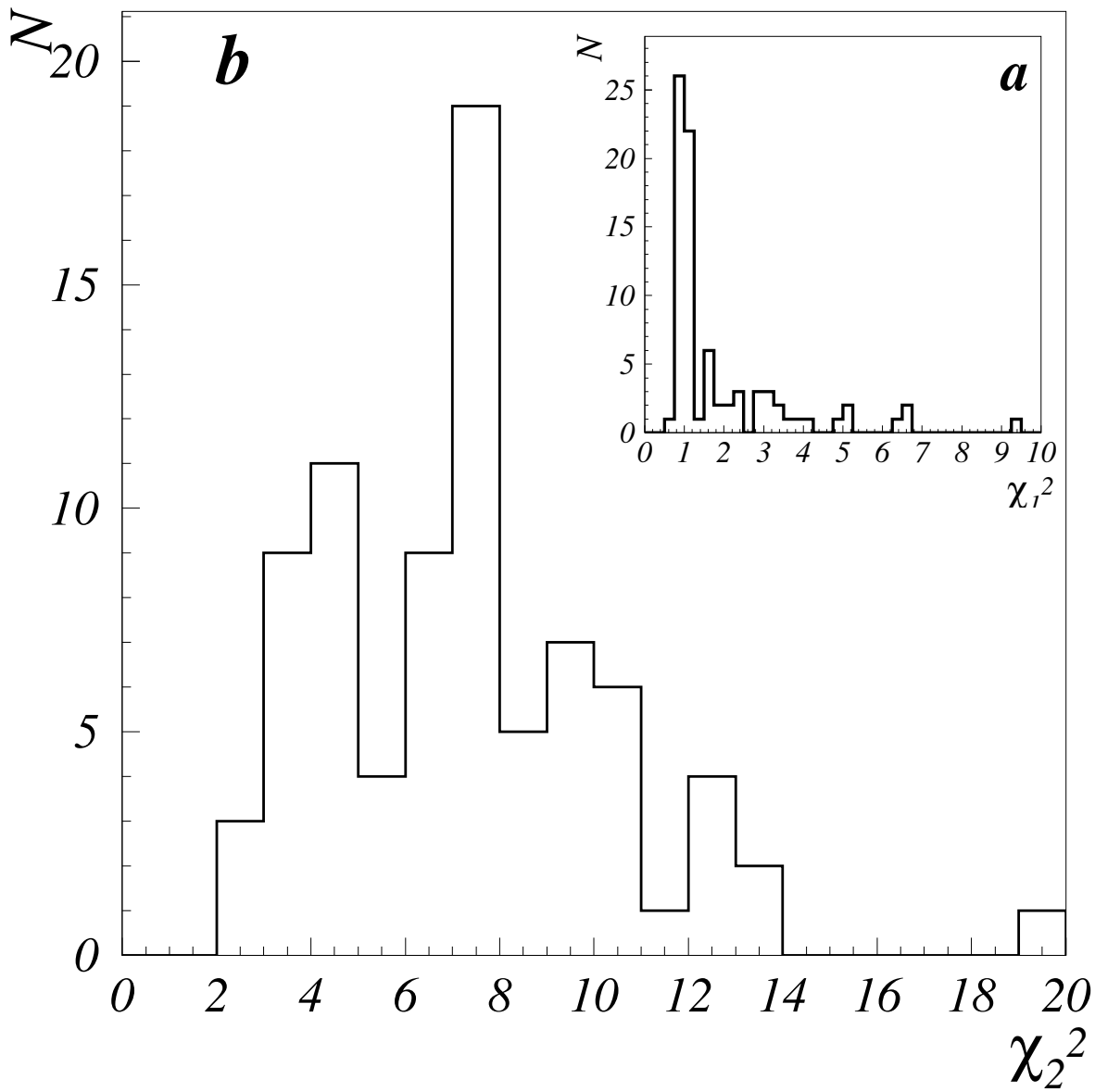

Figure 12: *Example MINUIT fits with 81 different correction factor combinations* $(A_{1k}, A_{2l}, A_{3m}, A_{4n})$. *In (a) the* χ^2 *values obtained for a particular* $< Q^2 >$ *region within a data sample; (b) the sum of the* χ^2 *from all the* Q^2 *regions analysed in the same sample.*

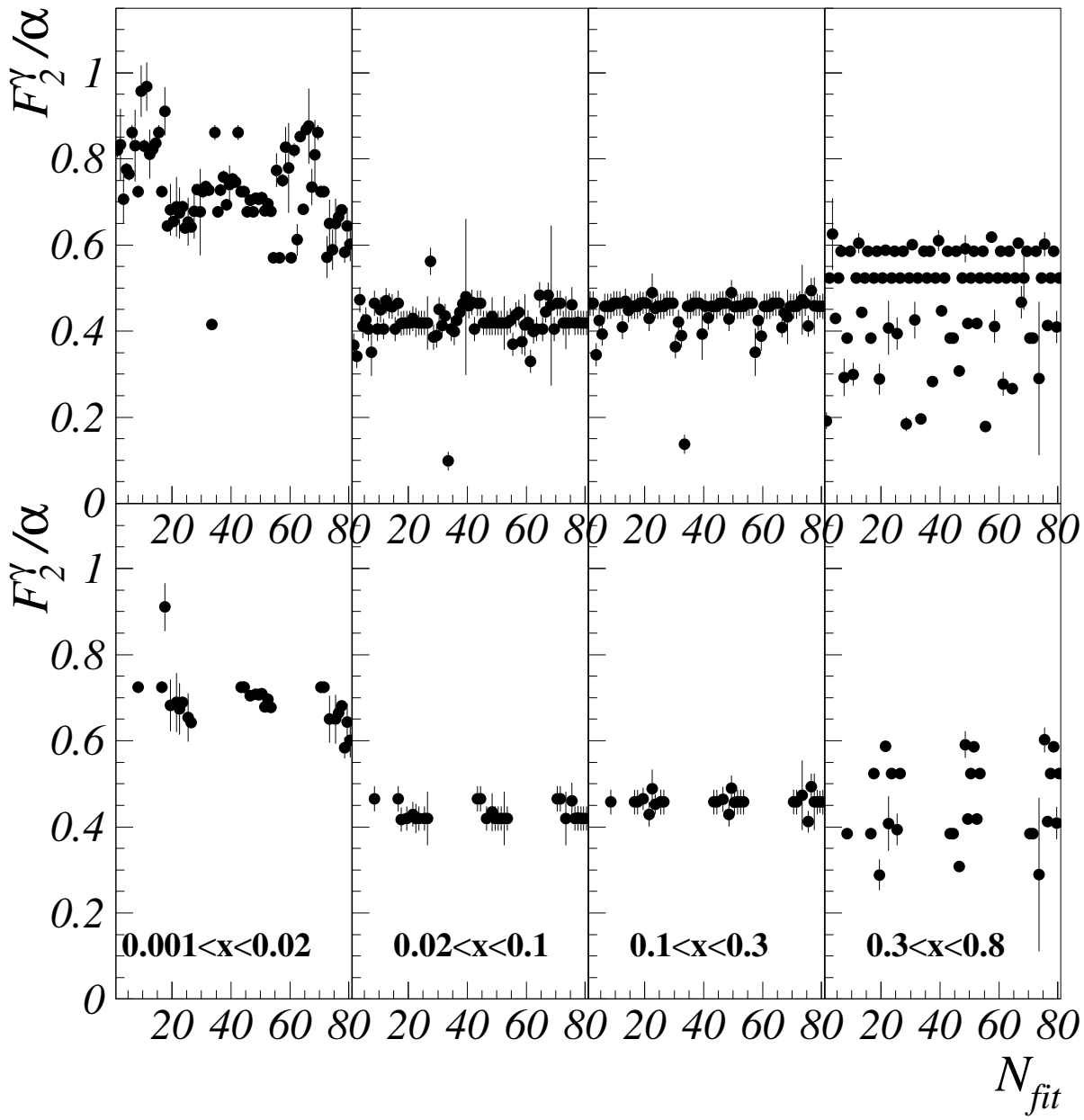

Figure 13: *Example of the measured F_2^γ in each of four x_{true} bins for the fits with different combinations of correction factors $A_{1k}, A_{2l}, A_{3m}, A_{4n}$. In the upper plots all fits are presented. In the lower plots only fits with $\chi^2 < \chi^2_{min} + 2$ are shown. Corrections have to be applied to such data before the results given in the tables are obtained.*

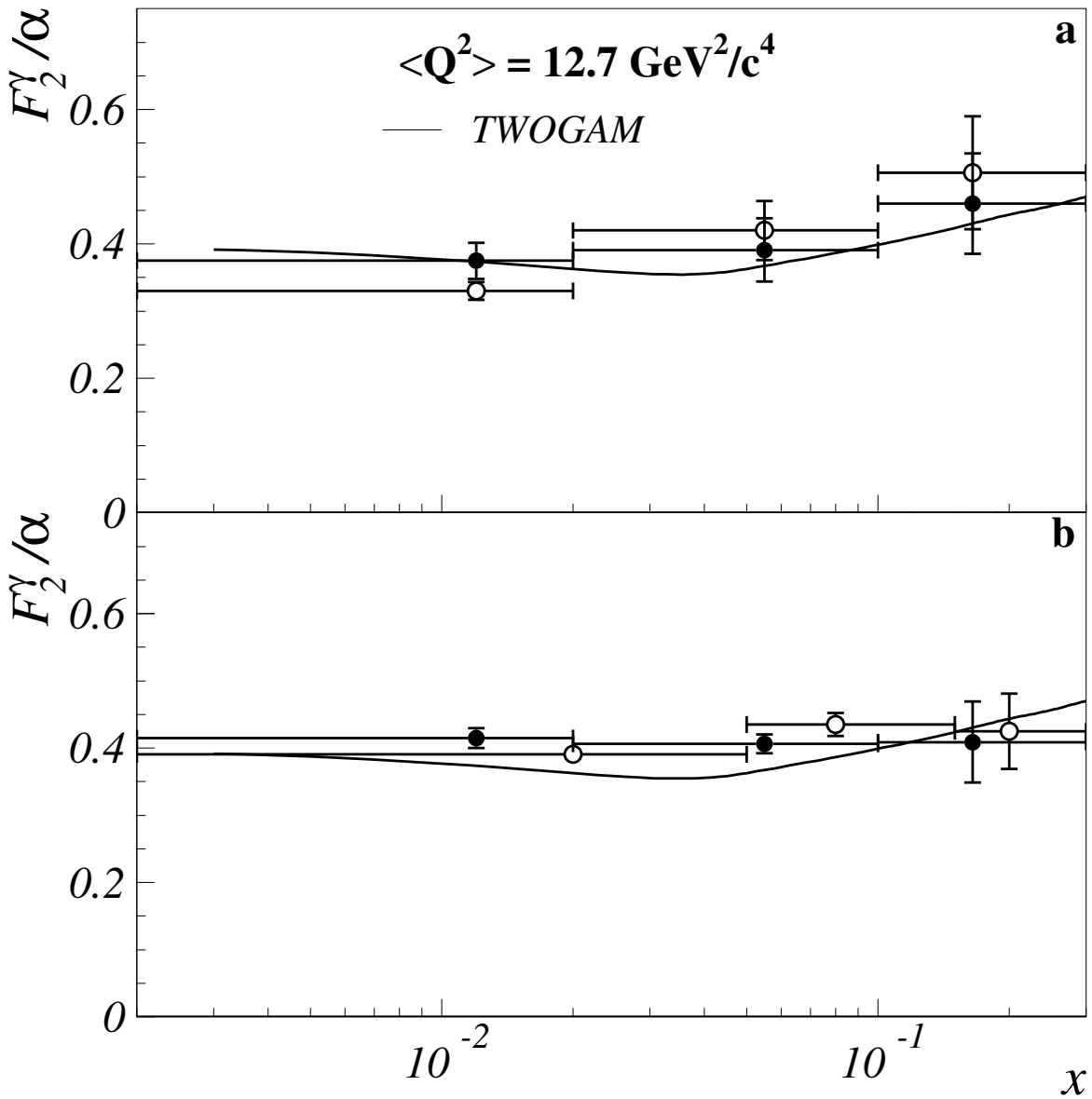

Figure 14: *Tests of (a) the MINUIT based procedure and (b) unfolding. a) Open circles: fit with the Monte Carlo sample treated as a sum of three components, black dots: the complete MINUIT fitting procedure. b) The results of the unfolding procedure in different x-bins. Open circles: bins proposed by the RUN program, black dots: bins identical to the ones used in the MINUIT procedure.*

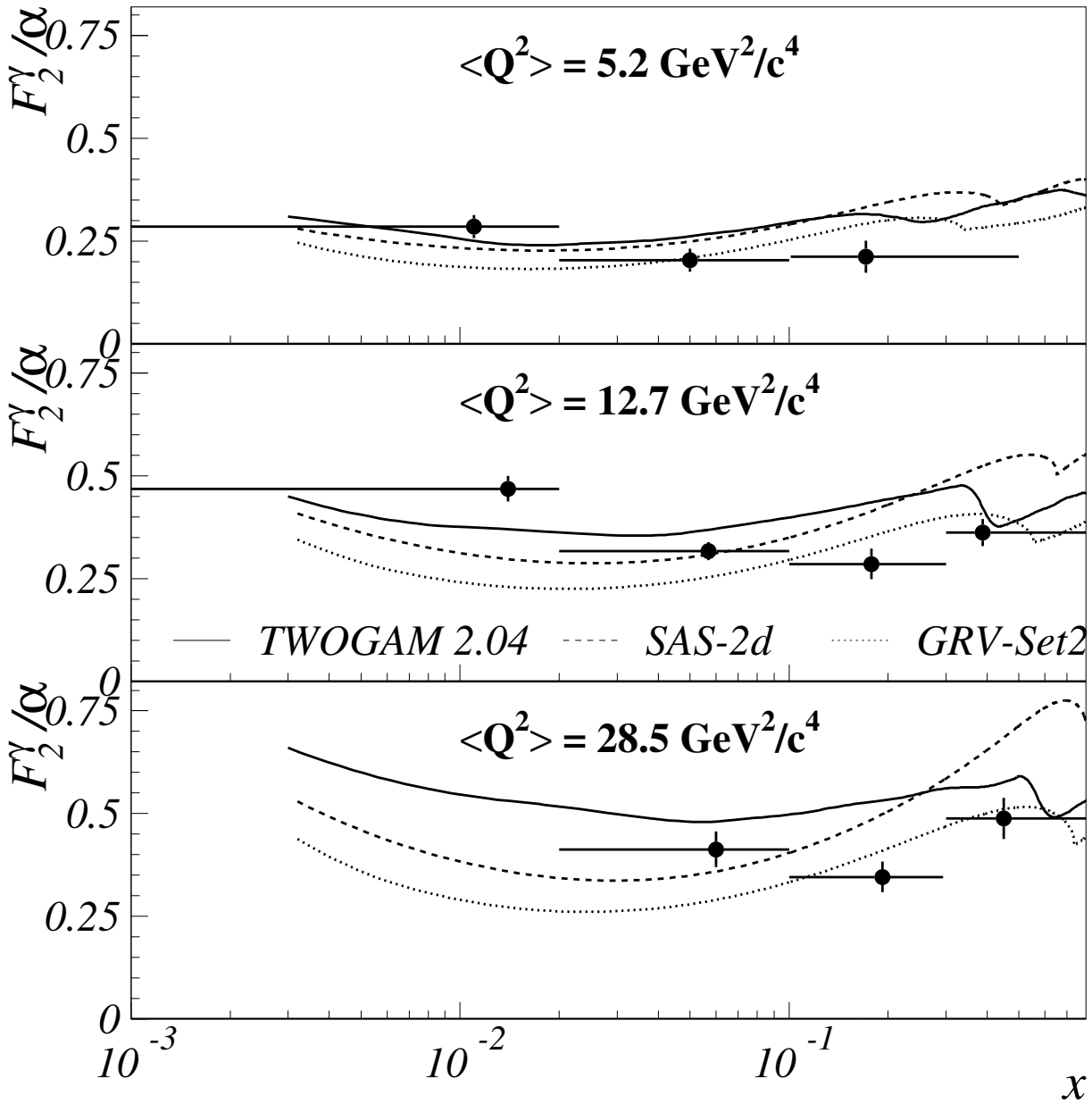

Figure 15: *The F_2^γ extracted from the LEP1 data at different $< Q^2 >$ as a function of x. Error bars show the total errors. The black points extracted from the data are compared with the predictions of the TWOGAM, GRV-Set2 and SaS-2d models.*

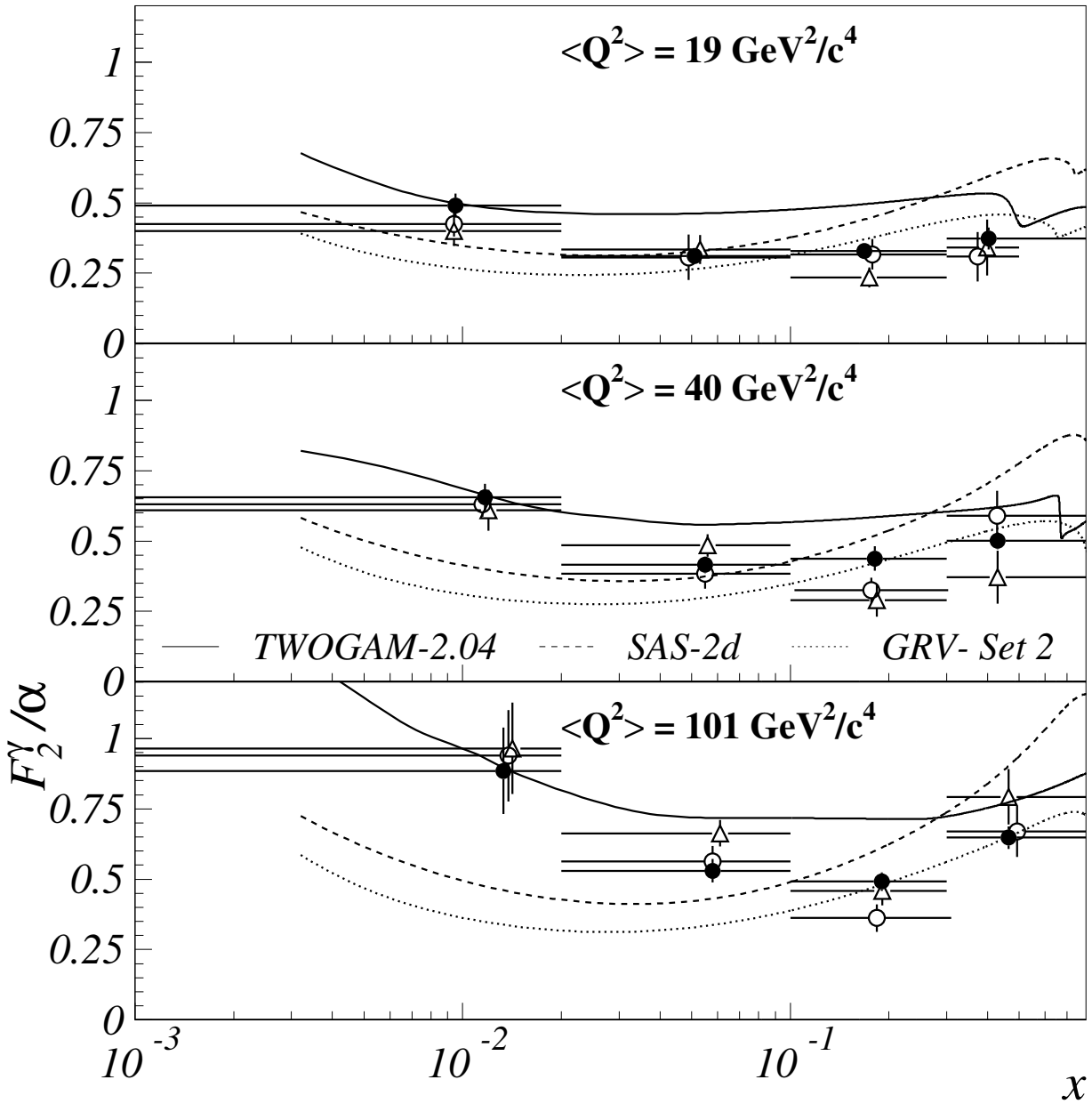

Figure 16: *F_2^γ extracted from the LEP2 data at different $< Q^2 >$ as a function of x. Error bars show total errors. The results extracted from the data using TWOGAM (black points), PHOJET (open circles), and PYTHIA (open triangles) are compared with the predictions of the TWOGAM, GRV-Set2 and SaS-2d models.*

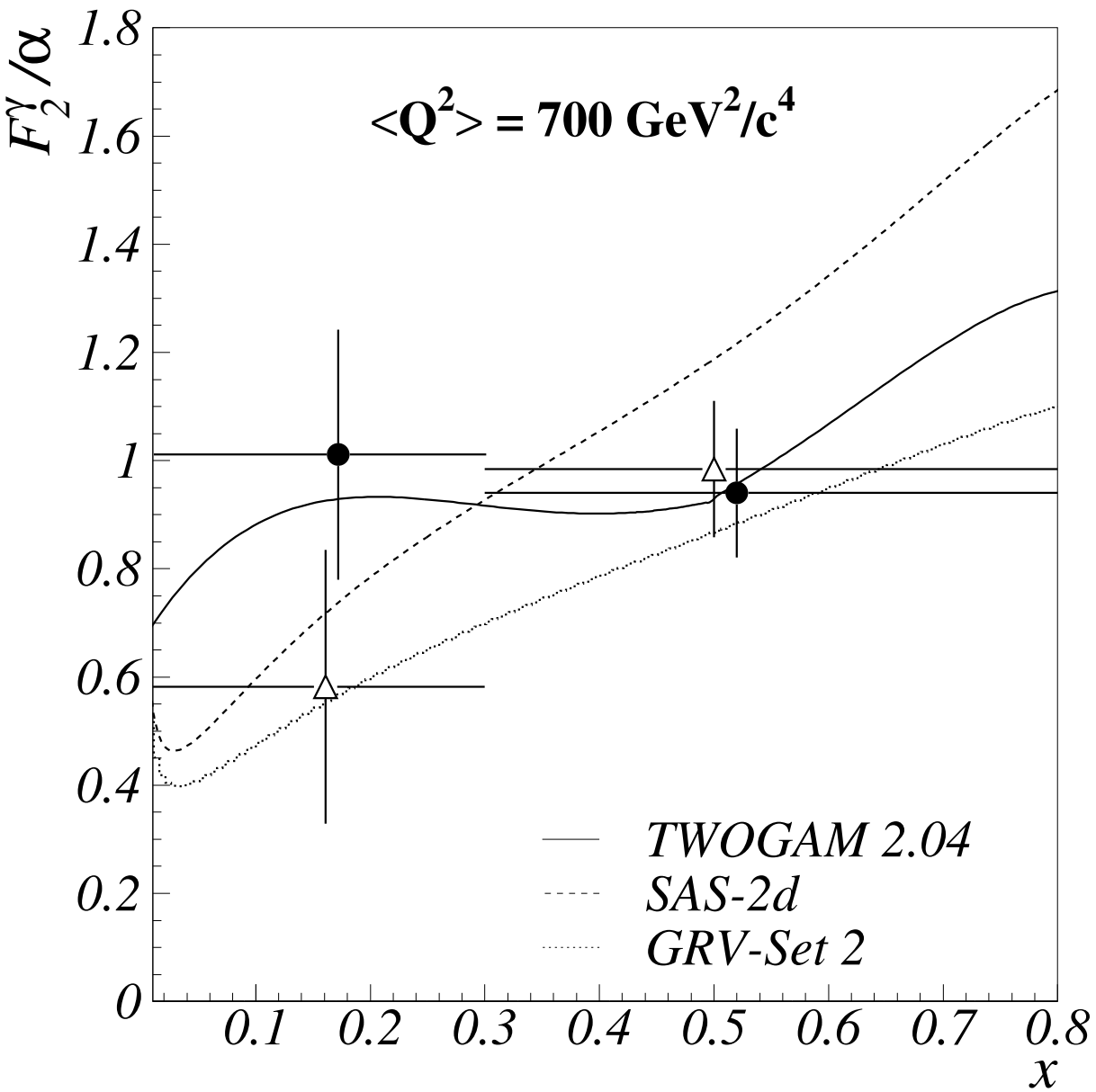

Figure 17: *F_2^γ extracted from the LEP2 FEMC tagged sample at $< Q^2 >$=700 GeV$^2/c^4$ as a function of x. Error bars show the total errors. The results extracted from the data using TWOGAM (black points) and PYTHIA (open triangles) are compared with the predictions of the TWOGAM, GRV and SaS models.*

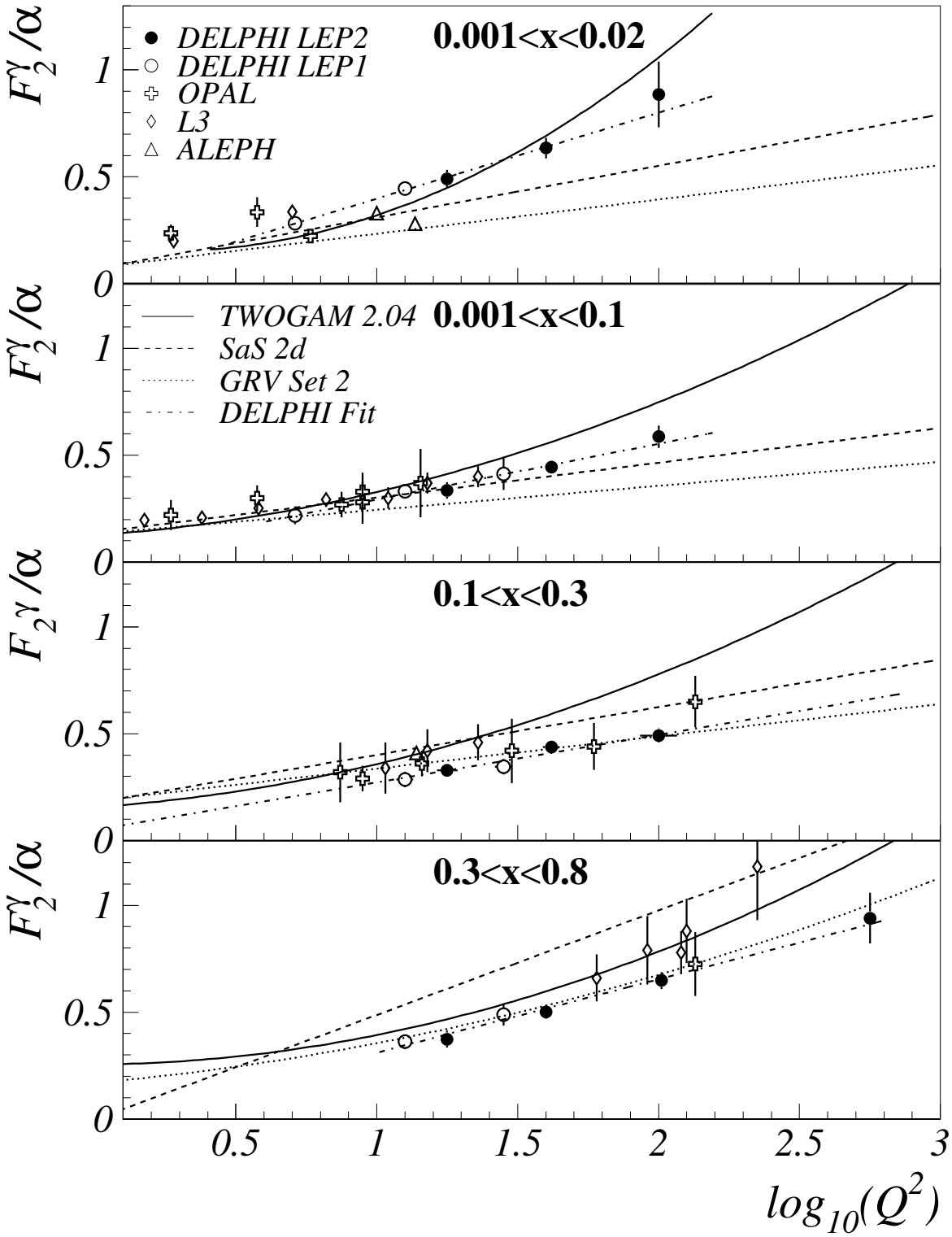

Figure 18: *The* $< F_2^\gamma >$ *in different* x *intervals as a function of* $< Q^2 >$ *compared with the predictions of the TWOGAM generator, the GRV and SaS models. The statistical and systematic errors are added in quadrature. The DELPHI points were extracted using TWOGAM; the data from other LEP experiments are presented when their measurements were made in similar* x *bins.*